NANOTECHNOLOGY AND SMARTPHONES ENABLE BETTER POINT OF CARE DIAGNOSTICS FOR KAPOSI'S SARCOMA HERPESVIRUS DNA

A Dissertation

Presented to the Faculty of the Graduate School

of Cornell University

In Partial Fulfillment of the Requirements for the Degree of

Doctor of Philosophy

by

Matthew Mancuso

May 2014

NANOTECHNOLOGY AND SMARTPHONES ENABLE BETTER POINT OF CARE DIAGNOSTICS FOR KAPOSI'S SARCOMA HERPESVIRUS DNA

Matthew Mancuso, Ph. D.

Cornell University 2013

In order to provide improved and more personalized medical care, better diagnosis and quantification of different biomarkers is necessary. During the tenure of my PhD I have created new systems for biodetection that exist at the interface of light and fluids, and that improve the sensitivity, scope, or some other aspect of the device. My first major research thrust was in the field of on-chip photonic resonators, where I increased the interaction between bioanalytes and light, enabling devices that were able to transduce up to a 40% increase in signal for a given amount of analyte. In my second work, I took an existing colorimetric gold nanoparticle reaction, multiplexed it for two targets using similar silver structures, and applied it to the differential diagnosis of Kaposi's sarcoma and Bacillary angiomatosis. My results indicate that the system created, without any optimization could detect DNA down to nanomolar levels, sufficient for use in the field. In my third, and penultimate piece of work, I created a smartphone based biosensor capable of quantifying the color change of my previous reaction, and extendable to many other systems, including colorimetric ELISAs. This sensor system is capable of detecting DNA from Kaposi's sarcoma associated herpesvirus, determining how much is present and uploading results to a

central server for later analysis. Taken together, over the course of my work I have created more sensitive and more multiplexed biosensors and shown how they can be connected to a smartphone for additional functionality.

BIOGRAPHICAL SKETCH

Matthew Mancuso was born in 1988 in Suffolk County, New York. He attended Stony Brook University from 2006-2009, earning a Bachelors of Engineering in Biomedical Engineering *cum laude*. During his time at Stony Brook University, he performed research under Professor Helmut Strey, working both at the university and at Brookhaven National Laboratories. In July 2009 he came to Cornell University to begin work on a PhD in Biomedical Engineering, under the supervision of Professor David Erickson in the Sibley School of Mechanical and Aerospace Engineering. His work at Cornell focused on using nanotechnology and smartphones to create novel diagnostic technologies. During his PhD, he was able to contribute work to the growing field of mobile health, showing how smartphones could play a pivotal role in the future of home medical care. Matthew has been named a Knight Nanotechnology Fellow, a National Science Foundation I-GERT Flexible Electronics Trainee, and a National Science Foundation Graduate Research Fellow. In addition to his academic work, Matthew co-founded vitaMe Technologies, a mobile health start-up, where he has worked to commercialize technologies developed by himself and his peers.

To my love Kathleen

ACKNOWLEDGMENTS

Isaac Newton once said that if he had seen further, it was because he stood on the shoulders of giants. While I may not see as far as Isaac Newton, if it weren't for a number of giants I wouldn't see at all. Thanks to all those who have helped me see.

First I would acknowledge my advisor, and more importantly, my mentor, Professor David Erickson. It was clear from the moment I met David that he was brilliant, enthusiastic, and passionate about what science. However, what became clear over the following 5 years was just how much more than that he could teach me. From lessons about success to finding happiness, David shared his own dreams with me, taught me the value of hard work, and left me always striving to be better. David, thank you for being a fantastic academic advisor and a fantastic role model.

Second, I'd like to thank my thesis committee. Professor Christopher Schaffer, you once lectured on how only a small percentage of our experiments should be successful; or we weren't attempting challenging enough things. I'll take this advice with me and make sure I'm always chasing after worthwhile goals. Professor Ober, thank you for providing insights into the future of material science and flexible sensors. Professor Cesarman, thank you for hosting me as a visiting student in NYC all those years ago. You've taught me that ultimately all problems we solve are human problems and that all technologies we create are used by and for them, a perspective that I lacked early in my engineering career.

Third, I would like to thank my colleagues at Cornell. The list of extraordinary people is too long to name all of you, but thank you. Thanks to Michael Mak, Xavier Serey, Dakota O'Dell, Seoho Lee, and Roanna Ruiz for all they've contributed to my

education and research. Also, thanks to Li Jiang and Vlad Oncescu, two friends who I've worked hand in hand with, who I've traveled the world with, and who I've learned so much about being a team with. I'd also like to thank Michael Kalontarov, who always kept me trying to be better.

Fourth, I'd like to thank my family. Mom, thank you for all that you've taught me, from teaching me to how to care about and love others, to showing me how to have the confidence to stand in front of anyone. The lessons you've taught me are too many to list, but I'm thankful for every single one. Dad, thank you for everything you've taught me about success and happiness. You've had a saying for nearly everything I've encountered in life from teaching me to "work smarter, not harder," when best utilizing time, to "avoiding snakes on the road and focusing on the bigger problem on the horizon," to something about a sheep. To my sister Michelle, my brother Michael, and my brother-in-law Eric, thank you for all the times you've been there for me, and for everything you've given to me, I love you all very much.

Fifth, to my second family, the Burkes. Thank you so much for everything you guys have contributed to my life. I'm blessed to have two extra parents and another set of sisters in my life. You and your relatives have taught me the meaning of the word family, and have been there for me through everything. Love you all.

And lastly of course, to my girlfriend of 6 years, Kathleen. I'll never be able to make up for all you've done for me, but I promise I'll try. From caring for me when I'm sick to all that you've taught me about hard work, you've contributed so much to my life. I'm still so blown away by your own research on breast cancer and am so proud of all you've done. You inspire me to be better every day. I love you.

TABLE OF CONTENTS

LIST OF FIGURES

LIST OF TABLES

CHAPTER 1

1. Introduction

1.1 Past, Present, and Future Medical Diagnosis

For many people the scariest moments of their lives will be learning of health complications in themselves and their loved ones. Spending most of their lives being generally healthy, patients show up at the doctor with only minor symptoms, and begin the process of uncovering what is wrong. Often times this process begins with a familiar physical examination, and ends with a simple prescription of antibiotics, or an order to rest for a few days. Other times, this diagnostic routine goes further, as more information is needed, and newer and more sensitive measures are ordered.

The earliest written records of medical diagnosis date back over four thousand years ago to the Egyptians and Greeks [1], though most of what is known today can be attributed to scientific developments of the last century. In these last hundred years or so, doctors began applying scientific and statistical methods in large scales to the study of the disease (i.e. the first double blind study in 1943 [2]), have categorically classified all different types of abnormalities[3] , and have developed treatments and therapeutics for many of the worst diseases facing human development [4]. New tools have been developed enabling doctors to detect rarer molecules and cells at increasing sensitivities, to see inside patients in a dozen different ways, and to detect subtleties that have often only just been discovered.

Importantly, many of the advances of the last century were made building off of similar breakthroughs in fields like electronics, chemistry, and physics. These new tools, treatments and ideas have been unarguably successful, increasing the average person's life expectancy by decades, and helping improve their quality of life significantly. They've taken advantage of our greatly increased scientific knowledge, and allowed us to save and improves lives in ways we couldn't have imagined a century before. They've also mirrored the dynamics of the time, favoring large centralized hubs to take advantage of economies of scale, and centralizing much of our medical expertise.

Overall, the state of advanced medical diagnosis today is not fundamentally different from the state of computation at the beginning of our information age. The vast amount of our capability is confined to central locations, and largely utilized only by professionals in the field. Only through these gatekeepers can an average person learn more about their health status. Just like with computers, having these centralized facilities is a significant improvement over not having them, but even greater advantages can be realized as some of these diagnostics are distributed to the ultimate end user, patients.

By decentralizing at least the first level of diagnostic tests, simple blood, urine, and saliva tests, and things which can be done by physical examination, it could be possible to provide better healthcare at less cost. Some examples already exist, including home pregnancy tests and home HIV tests. With over 4 million births a year and total revenues of over $220M, it's easy to imagine the impact of home pregnancy tests on medical care [5]. Home HIV saliva tests, just approved in May 2013, will

hopefully have a similar effect. Glucose monitors used by diabetes go a step further, not only reducing the cost of providing care, but enabling many diabetics to live otherwise normal lives, a reality that would be difficult without such technologies. In addition to these technologies, home health monitoring exists for cholesterol, urine tests, and a number of other applications, all with some level of success.

Together, these two devices, home pregnancy tests and glucose monitors, also illustrate a key difference between two types of medical diagnostics: qualitatively read binary tests and quantitative tests which require additional hardware. While tests strips such as pregnancy tests have seen some success reaching home markets, quantitative tests have had a much harder time finding widespread adoption, with glucose tests being the exception, rather than the rule. Mainly this problem is caused by the cost of the hardware required to read out tests, and the infrequency which medical tests are required by generally healthy people. Making an analogy to the well known razor-razorblade business model in which razors are sold cheap to drive the sales of blades, for individual health problems often the cost of the "razor" can't be amortized over enough "blades."

This problem can be solved by creating a platform that combines many different health tests and only a single reader. A single diagnostic platform that ultimately connects many tests could provide an unprecedented ability to monitor patient's health in real time, explain the results in a meaningful way to the patient, communicate results to the doctor, and provide better care at both the patient and population level. Importantly, such a device would ultimately share many characteristics with one of the most important technologies of this decade, the smartphone.

1.2 The Smartphone Revolution

It's extraordinary when a single technology comes along which changes the way people all over the developed world go about their daily lives. Almost 46% of American adults have a smartphone today and by 2016 an anticipated 250 million smartphones will be in use US[6]. Smartphones are used to obtain information and for entertainment, financial transactions, photography, exercise, and most recently and relevantly, for healthcare.

Already, commercial healthcare applications exist including well known include exercise and fitness monitoring applications [7-9], as well as vaccine logs [10], sleep monitoring applications [11], diagnosis decision support apps [12], and applications that can be used to image and diagnose skin cancer [13]. Additionally, smartphones accessories exist that can collect heart rate [14], blood pressure [15], and blood oxygen saturation [16]. Together, the total smartphone based healthcare was worth $1.3 billion in 2011, up nearly twice its 2010 value, and is expected to continue growing rapidly [17].

Importantly however, all these existing commercial smartphone based systems rely on user input or physical measurements (e.g. blood pressure, heart rate) that are generally non-specific vital signs and were simply commercialized first because they are easy to obtain. What remains to be done is quantitative monitoring of different pathogens and antigens in bodily fluids such as sweat, saliva, urine, and blood, all of which contain a tremendous amount of health information. As explained in 1.1, these quantitative signals are often the most difficult to measure at home, and so far, have

been only marginally successful. Obtaining numerical health information like this, such as cholesterol and vitamin levels, has been one aim in our broader body of work.

Looking elsewhere, if the development of the smartphone has caused extraordinary change in the developed world, its introduction into developing nations has been nothing short of profound. While personal computers proved too expensive to reach some locations, cell phones are thriving in locations where electricity is often periodic, and serving as the primary means of internet access in these locations. In areas such as India and Africa, cell phones have already revolutionized how people contact each other, share information, and even pay for things. In 2011, over 60% of Africans, or 600 million customers, had access to cell phones, with predictions expecting over 80% penetration by 2014 [18]. Smartphone penetration is picking up at an incredible rate, with approximately 100M connections in 2013, and predictions of over 230M connections in 2015.

Importantly, in these locations smartphones have reached places where developed world healthcare haven't. Not only can smartphones act as a gatekeeper for further healthcare, in these locations, smartphone based diagnostics can help provide a level of care that wasn't previously possible. By connecting new diagnostic tests to the communications capabilities of smartphones, more advanced technologies can be deployed, and doctor's opinions can even be brought in to make life saving decision in locations too remote for hospital care.

1.3 Kaposi's sarcoma, an infectious disease and a lens for diagnostic development

One condition where better diagnostics are drastically needed is in the case of Kaposi's sarcoma (KS) in sub-Saharan Africa. Perhaps KS is best known in the developed world for its relationship with the onset of the acquired immunodeficiency syndrome (AIDS) epidemic in the early 1980s. As patients presented at the hospital with AIDS, often their first symptom was the presence of red skin lesions, a symptom not of AIDS, but actually of KS, an opportunistic disease [19-22]. During the following years, significant research efforts were made to determine the cause of AIDS, leading to the discovery of HIV in 1983 [23-24]. A little over ten years later the cause of KS was first connected to a second virus, Kaposi's sarcoma-associated herpesvirus (KSHV), later given the alternative designation of human herpesvirus 8 (HHV-8) [25].

KS is the most prevalent cancer faced by HIV-infected individuals not on therapy. Initial studies showed that it affected 1 in 20 HIV-positive patients [26]. Highly active anti-retroviral therapy (HAART) has improved the outlook for patients in the developed world, but even here it remains increased in incidence as compared to the pre-AIDS era [27-28]. In Sub-Saharan Africa, both HIV and KS are endemic, and KS is the fourth leading cancer in the region [29]. In Uganda, KS is the number one cause of cancer in men [29-30].

In some locations KSHV rapidly spreads, presumably through saliva [31-33], and, reaches seroprevalence of over half the population [29, 34]. KSHV, similar to the better known herpesviruses HSV-1 and HSV-2 (oral and genital herpes) can establish

a latent infection, and remains without causing any disease for the remaining life in most infected hosts, being necessary but not sufficient of KS development (the other condition required being a weakened immune system). In locations where the seroprevalence of KSHV is high, the clinically relevant test becomes determining if KSHV is present in a specific tumor, and not simply if it is present in a person's blood. Further, this requirement can lead to determining if a significantly high enough concentration of KSHV is present, as even seroprevalent virus can cause a PCR to come back positive from blood in the biopsy sample.

In addition to the requirement for sensitive quantitative detection, an additional challenge presents itself in the diagnosis of KS in the form of similarly presenting diseases. KS shares a similar presentation and many other histological features with a number of diseases including bacillary angiomatosis (BA) caused by Bartonella henselae or quintana, and pyogenic granuloma. Taken together, these two challenges require any diagnostic for KS to be both sufficiently sensitive and resolved enough to separate seroprevelance from actual infection, and to separate KS from other infectious conditions.

In hospitals, these problems are solved and KS diagnostic often takes the form of skin biopsies processed for histology using instruments like tissue processing systems and microtomes, and stains including not only H&E but also more advanced immunohistochemistry specific for unique KSHV proteins. In cases where a diagnosis still isn't certain, polymerase chain reaction (PCR) specific for unique KSHV DNA sequences can also be used to confirm a diagnosis. However, these techniques often aren't available in the developing world, and certainly aren't available or translatable

to point of care setting.

While a point of care diagnostic for KS could revolutionize care in sub-Saharan Africa, these two challenges present themselves in the creation of point-of-care diagnostics. Additionally, all of the hardware necessary to process a biopsy samples must in some way be built into a diagnostic test.

1.4 Point of Care Biosensors in the Literature

Already, a tremendous amount of work has been done on developing point of care biosensors. Devices have been constructed using mechanical [35-36], electrical [37], and optical [38] techniques to detect bioanalytes in minute quantities. Often these devices combine microfluidics and other nanotechnologies in order to create tools which both operate at the length scale of the detection target and at a macroscopic scale which can be simply read-out. Some examples have also been applied in developing world settings, where the additional constraints of a lack of resources and trained personnel complicate matters [39-40].

One interesting example is that of on-chip optical resonators. Optical devices are particularly interesting due to their high sensitivity, their capacity for multiplexed detections, and their ability to operate interface well with bioanalytes in an aqueous solution[41-46]. In the literature, many different optically resonant architectures have been studied including photonic crystals [38, 47], microtoroids [48], and microring/microracetracks [49-50]. In chapter 1 we construct an optically resonant microring, and demonstrate how improvements can be made by increasing bioanalyte-

core waveguide energy interactions.

Another interesting example which is investigated more in Chapter 3 is that of biosensors which link a biodetection reaction to a colorimetric nanoparticle aggregation reaction [51-53]. These reactions are particularly interesting because of the simplicity with which they can be read out. Compared to the previously mentioned class of waveguiding biosensors, these devices require significantly reduced external equipment, yet exploit similar resonant techniques to achieve high sensitivities [51, 54-55] Some works have even shown detection of unamplified DNA [53]. In Chapter 4 we develop our own multiplexed version of such a system, traditionally something which has proved challenging to accomplish.

A third class of biosensor, only very recently making their introduction in the last decade, is that which connects a bioanalyte detection reaction to something that can be read out in a smartphone. These tests are particularly useful because of the ubiquity with which smartphones not only exist in our lives, but with which people are familiar using them. By connecting a complex diagnostic test to an easy to use smartphone, systems can often be created that allow nontechnical audiences to complete difficult tasks.

Some of the earliest examples of these devices have come out of the Ozcan research group, where researchers developed field portable microscopes based on camera phones [56-59]. Additional works have connected colorimetric test strip reactions to smartphones to enable reading out things like pH[60], urine tests [61], and cholesterol tests[62]. However, most of these early works use the smartphones camera, as opposed to a separate optical detector. While this has advantages in terms

of simplicity, because a medical device manufacturer has no control over the camera in a phone, or how to tell if it's damaged over its lifetime, it provides difficulty in producing repeatable measurements. In Chapter 4 we develop a system which attempts to solve this problem.

2. Research Overview and Dissertation Breakdown

In Chapter 2 of this dissertation, a look is taken at the creation of a more traditional optofluidics biosensor, based on waveguides and optical ring resonators. The novel device discussed in this chapter is made of polymer, rare for these devices, and is constructed in such a way that it is porous, one of the first of its kind. The additional porosity in the device creates more interaction between bioanalytes in the surrounding liquid cladding and the optical energy stored in the polymer waveguide. More uniquely, the structure allows the bioanalytes to directly enter the waveguide, and interact with the optical energy where it is most concentrated. Together, these effects allow for a biosensor which is 40% more sensitive to changes in the refractive index of the cladding solution than a polymer device alone. These improvements to sensitivity are significant, and due to the method of fabrication and materials used, devices such as the ones in this work could one day potentially see use in a number of different medical sensors.

In Chapter 3, a first look is taken at creating a diagnostic for KSHV in the developing world. In this work, a novel system of nanoparticles is created capable of making the differential diagnosis of KSHV and BA using two different colorimetric

reactions. The system builds on other nanoparticle work for a single target, and shows how a colorimetrically multiplexed system can be created. By monitoring multiple color changes, more information can be determined from a single sample collection.

In Chapter 4, a smartphone platform capable of reading out the colorimetric test from Chapter 2 is developed. The accessory plugs into the µUSB port of an Android smartphone, and uses the power, communications, and connectivity of the phone to create a novel biosensor platform. In this chapter we detail the creation of the device, and show how samples of KSHV DNA can be detected in microfluidic chips. Further, we characterize the resolution and sensitivity of the device.

Lastly, in chapter 5, I review the accomplishments in this work and provide perspective for where the future of the work could go. I hope that over the course of this work a clear change can be seen in how biosensors advance from complicated laboratory devices to simple smartphone accessories, completing the same tasks with similar sensitivity. It's my hope that in the future many medical diagnostics will share this same transition, and enable people to cheaply and easily run to the pharmacy and purchase tests providing a wealth of physiologic information.

3. References

1. Berger, D., *A brief history of medical diagnosis and the birth of the clinical laboratory. Part 1--Ancient times through the 19th century.* MLO Med Lab Obs, 1999. **31**(7): p. 28-30, 32, 34-40.
2. D'Arcy Hart, P., *A change in scientific approach: from alternation to randomised allocation in clinical trials in the 1940s.* BMJ, 1999. **319**(7209): p. 572-3.
3. *History of the development of the ICD*. World Health Organization 2014; Available from: http://www.who.int/classifications/icd/en/HistoryOfICD.pdf.
4. Bhatt, A., *Evolution of clinical research: a history before and beyond james lind.* Perspect Clin Res, 2010. **1**(1): p. 6-10.
5. Moldvay, C., *Pregnancy Test Kit Manufacturing*, in *IBIS World Reports*. 2012
6. (2012) *Pew Internet and American Life Project.* *http://pewresearch.org/pubs/2206/smartphones-cell-phones-blackberry-android-iphone*.
7. Nike. *Nike Plus*. 2012; Available from: http://nikeplus.nike.com/plus/.
8. Inc., H. *iFitnessPro*. 2012; Available from: http://www.healthxperts.net/.
9. MapMyFITNESS, I. *MapMyRun*. 2012; Available from: https://www.mapmyrun.com/.
10. Smartware, I. *Vaccination Record*. 2012; Available from: http://www.smartware.com/android/vacrec/index.html.
11. Labs, M.D. *Sleep Cycle*. 2009; Available from: http://www.sleepcycle.com/.
12. Healthcare, I. *Differential Diagnosis Support*. 2012; Available from: www.isabelhealthcare.com/.
13. Labs, C. *SkinScan*. 2012; Available from: http://www.skinscanapp.com/.

14. Inc., A. *Instant Heart Rate*. 2012; Available from: http://www.azumio.com/apps/heart-rate/.

15. iHealth. *Blood Pressure Dock*. 2012; Available from: http://www.ihealth99.com/BP3_feature.html.

16. Schultz, M., *Hemoglobe*. 2012.

17. research2guidance, *Mobile Health Market Report 2011-2016: The impact of smartphone applications on the mobile health industry*. 2012.

18. *African Mobile Observatory 2011*. 2014, Groupe Speciale Mobile (GSM).

19. Hymes, K.B., et al., *Kaposi's sarcoma in homosexual men-a report of eight cases.* Lancet, 1981. **2**(8247): p. 598-600.

20. Friedman-Kien, A.E., *Disseminated Kaposi's sarcoma syndrome in young homosexual men.* J Am Acad Dermatol, 1981. **5**(4): p. 468-71.

21. Pitchenik, A.E., et al., *Opportunistic infections and Kaposi's sarcoma among Haitians: evidence of a new acquired immunodeficiency state.* Ann Intern Med, 1983. **98**(3): p. 277-84.

22. *Update on Kaposi's sarcoma and opportunistic infections in previously healthy persons--United States.* MMWR Morb Mortal Wkly Rep, 1982. **31**(22): p. 294, 300-1.

23. Gallo, R.C., et al., *Isolation of human T-cell leukemia virus in acquired immune deficiency syndrome (AIDS).* Science, 1983. **220**(4599): p. 865-7.

24. Barre-Sinoussi, F., et al., *Isolation of a T-lymphotropic retrovirus from a patient at risk for acquired immune deficiency syndrome (AIDS).* Science, 1983. **220**(4599): p. 868-71.

25. Chang, Y., et al., *Identification of herpesvirus-like DNA sequences in AIDS-associated Kaposi's sarcoma.* Science, 1994. **266**: p. 1865-1869.

26. Gallo, R.C., *The enigmas of Kaposi's sarcoma.* Science, 1998. **282**(5395): p. 1837-9.

27. Nguyen, H.Q., et al., *Persistent Kaposi sarcoma in the era of highly active antiretroviral therapy: characterizing the predictors of clinical response.* AIDS, 2008. **22**(8): p. 937-45.

28. Eltom, M.A., et al., *Trends in Kaposi's sarcoma and non-Hodgkin's lymphoma incidence in the United States from 1973 through 1998.* J Natl Cancer Inst, 2002. **94**(16): p. 1204-10.

29. Ferlay J, et al. *Cancer Incidence and Mortality Worldwide: IARC CancerBase No. 10 [Internet]*. GLOBOCAN 2008 v1.2 2010 [cited 2011 11/15/2011]; Available from: http://globocan.iarc.fr].

30. Jemal, A., et al., *Global cancer statistics.* CA: A Cancer Journal for Clinicians, 2011. **61**(2): p. 69-90.

31. Butler, L.M., et al., *Kaposi Sarcoma-Associated Herpesvirus (KSHV) Seroprevalence in Population-Based Samples of African Children: Evidence for At Least 2 Patterns of KSHV Transmission.* Journal of Infectious Diseases, 2009. **200**(3): p. 430-438.

32. Minhas, V., et al., *Early Childhood Infection by Human Herpesvirus 8 in Zambia and the Role of Human Immunodeficiency Virus Type 1 Coinfection in a Highly Endemic Area.* American Journal of Epidemiology, 2008. **168**(3): p. 311-320.

33. Martro, E., et al., *Comparison of human herpesvirus 8 and Epstein-Barr virus seropositivity among children in areas endemic and non-endemic for Kaposi's sarcoma.* Journal of Medical Virology, 2004. **72**(1): p. 126-131.

34. He, J., et al., *Seroprevalence of human herpesvirus 8 among Zambian women of childbearing age without Kaposi's sarcoma (KS) and mother-child pairs with KS.* J Infect Dis, 1998. **178**(6): p. 1787-90.

35. Arlett, J.L., E.B. Myers, and M.L. Roukes, *Comparative advantages of mechanical biosensors.* Nat Nano, 2011. **6**(4): p. 203-215.

36. von Muhlen, M.G., et al., *Label-Free Biomarker Sensing in Undiluted Serum with Suspended Microchannel Resonators.* Analytical Chemistry, 2010. **82**(5): p. 1905-1910.

37. Zheng, G., X.P.A. Gao, and C.M. Lieber, *Frequency Domain Detection of Biomolecules Using Silicon Nanowire Biosensors.* Nano Letters, 2010. **10**(8): p. 3179-3183.

38. Mandal, S., J.M. Goddard, and D. Erickson, *A multiplexed optofluidic biomolecular sensor for low mass detection.* Lab on a Chip, 2009(DOI: 10.1039/b907826f).

39. Chin, C.D., et al., *Microfluidics-based diagnostics of infectious diseases in the developing world.* Nat Med, 2011. **17**(8): p. 1015-1019.

40. Martinez, A.W., et al., *Diagnostics for the Developing World: Microfluidic Paper-Based Analytical Devices.* Analytical Chemistry, 2009. **82**(1): p. 3-10.

41. Yariv, A., *Universal relations for coupling of optical power between microresonators and dielectric waveguides.* Electronics Letters, 2000. **36**(4): p. 321-322.

42. Yariv, A., *Critical coupling and its control in optical waveguide-ring resonator systems.* Ieee Photonics Technology Letters, 2002. **14**(4): p. 483-485.

43. Seo, B.J., et al., *Design of ring resonators using electro-optic polymer waveguides.* Journal of Physical Chemistry C, 2008. **112**(21): p. 7953-7958.

44. Xu, D.X., et al., *Folded cavity SOI microring sensors for high sensitivity and real time measurement of biomolecular binding.* Optics Express, 2008. **16**(19): p. 15137-15148.

45. Chao, C.Y. and L.J. Guo, *Polymer microring resonators fabricated by nanoimprint technique.* Journal of Vacuum Science & Technology B, 2002. **20**(6): p. 2862-2866.

46. Chao, C.Y., W. Fung, and L.J. Guo, *Polymer microring resonators for biochemical*

sensing applications. IEEE Journal of Selected Topics in Quantum Electronics, 2006. **12**(1): p. 134-142.

47. Mandal, S. and D. Erickson, *Nanoscale Optofluidic Sensor Arrays.* Optics Express, 2008. **16**(3): p. 1623-1631.

48. Martin, A.L., et al., *Replica-molded high-Q polymer microresonators.* Optics Letters, 2004. **29**(6): p. 533-535.

49. Myers, F.B. and L.P. Lee, *Innovations in optical microfluidic technologies for point-of-care diagnostics.* Lab on a Chip, 2008. **8**(12): p. 2015-2031.

50. De Vos, K., et al., *SOI optical microring resonator with poly(ethylene glycol) polymer brush for label-free biosensor applications.* Biosensors & Bioelectronics, 2009. **24**(8): p. 2528-2533.

51. Rosi, N.L. and C.A. Mirkin, *Nanostructures in Biodiagnostics.* Chemical Reviews, 2005. **105**(4): p. 1547-1562.

52. Yanik, A.A., et al., *Seeing protein monolayers with naked eye through plasmonic Fano resonances.* Proceedings of the National Academy of Sciences, 2011.

53. Storhoff, J.J., et al., *Homogeneous detection of unamplified genomic DNA sequences based on colorimetric scatter of gold nanoparticle probes.* Nat Biotech, 2004. **22**(7): p. 883-887.

54. Reynolds, R., C.A. Mirkin, and R.L. Letsinger, *Homogeneous, Nanoparticle-Based Quantitative Colorimetric Detection of Oligonucleotides.* J. Am. Chem. Soc, 2000. **122**: p. 3795-3796.

55. Thompson, D.G., et al., *Ultrasensitive DNA Detection Using Oligonucleotide−Silver Nanoparticle Conjugates.* Analytical Chemistry, 2008. **80**(8): p. 2805-2810.

56. Greenbaum, A., et al., *Wide-field computational color imaging using pixel super-resolved on-chip microscopy.* Opt. Express, 2013. **21**(10): p. 12469-12483.

57. Greenbaum, A., U. Sikora, and A. Ozcan, *Field-portable wide-field microscopy of dense samples using multi-height pixel super-resolution based lensfree imaging.* Lab on a Chip, 2012. **12**(7).

58. Isikman, S.O., et al., *Field-portable lensfree tomographic microscope.* Lab on a Chip, 2011. **11**(13): p. 2222-2230.

59. Lee, M., O. Yaglidere, and A. Ozcan, *Field-portable reflection and transmission microscopy based on lensless holography.* Biomed. Opt. Express, 2011. **2**(9): p. 2721-2730.

60. Oncescu, V., D. O'Dell, and D. Erickson, *Smartphone based health accessory for colorimetric detection of biomarkers in sweat and saliva.* Lab on a Chip, 2013. **13**(16): p. 3232-3238.

61. Shen, L., J.A. Hagen, and I. Papautsky, *Point-of-care colorimetric detection with a smartphone.* Lab on a Chip, 2012. **12**(21): p. 4240-4243.

62. Oncescu, V., M. Mancuso, and D. Erickson, *Cholesterol testing on a smartphone.* Lab on a Chip, 2014. **14**(4): p. 759-763.

CHAPTER 2

NANOPOROUS POLYMER RING RESONATORS FOR BIOSENSING

Optically resonant devices are promising as label-free biomolecular sensors due to their ability to concentrate electromagnetic energy into small mode volumes and their capacity for multiplexed detection. A fundamental limitation of current optical biosensor technology is that the biomolecular interactions are limited to the surface of the resonant device, while the highest intensity of electromagnetic energy is trapped within the core. In this paper, we present nanoporous polymer optofluidic devices consisting of ring resonators coupled to bus waveguides. We report a 40% increase in polymer device sensitivity attributed to the addition of core energy- bioanalyte interactions.

Mancuso, M., Goddard, J., Erickson, D. "Nanoporous Polymer Ring Resonators for Biosensing" *Optics Express* 20, 1, 245-255 (2012). Reproduced with permission of the Optics Society of America

1. Introduction

Label-free biosensors are a promising class of biomolecular detectors because they bypass the need for a fluorescent, radio, or enzymatic label. Dependence on such a label to detect a biomolecular interaction can adversely impact device performance, either by interfering with the binding event (false negative) or by non-specific adsorption of the labeling molecule (false positive) [1]. There are a number of well developed techniques that permit direct label-free detection of bound target biomolecules [2], including optical [3-5], electrical [6], and acoustic sensors [7]. Within the broader class of label-free biosensors, optically resonant devices are particularly promising due to their ability to concentrate electromagnetic energy into small mode volumes, their capacity for multiplexed detections, and their ability to operate in aqueous environments [8-13]. A number of different architectures have been investigated in the development of optically resonant biosensors, including photonic crystals [5, 14], microtoroids [15], and microring/microracetracks [16-17].

A fundamental limitation to the sensitivity of most optical biosensors is that the biomolecular interactions are limited to the surface of the resonant device, while the highest intensity of electromagnetic energy is trapped within the core (Fig 1a). An example of a technique that attempts to resolve this problem are liquid core slot waveguide biosensors, which confine both the target bioanalyte and optical energy to the same volume [18]. These types of devices can also be fabricated into ring resonators to further localize optical energy [19], yet their commercialization is often hindered by expensive and complicated fabrication.

At the other end of the spectrum, polymer optical biosensors offer low cost, simple fabrication, but suffer from lower sensitivities than silicon equivalents [10, 12-13, 20-22]. Polymers are commercially available with a range of thermal, mechanical, and optical properties,

and can be readily functionalized for the immobilization of biomolecular sensing agents [23]. Further, Polymer chemistry can be tuned to yield unique optical structures and properties that are difficult to fabricate with traditional silicon based techniques. Due to their cheap material and fabrication requirements polymer biosensors lend themselves well to being manufactured as one-use disposables. Because of this, problems with surface fouling due to repeated use can often be mitigated.

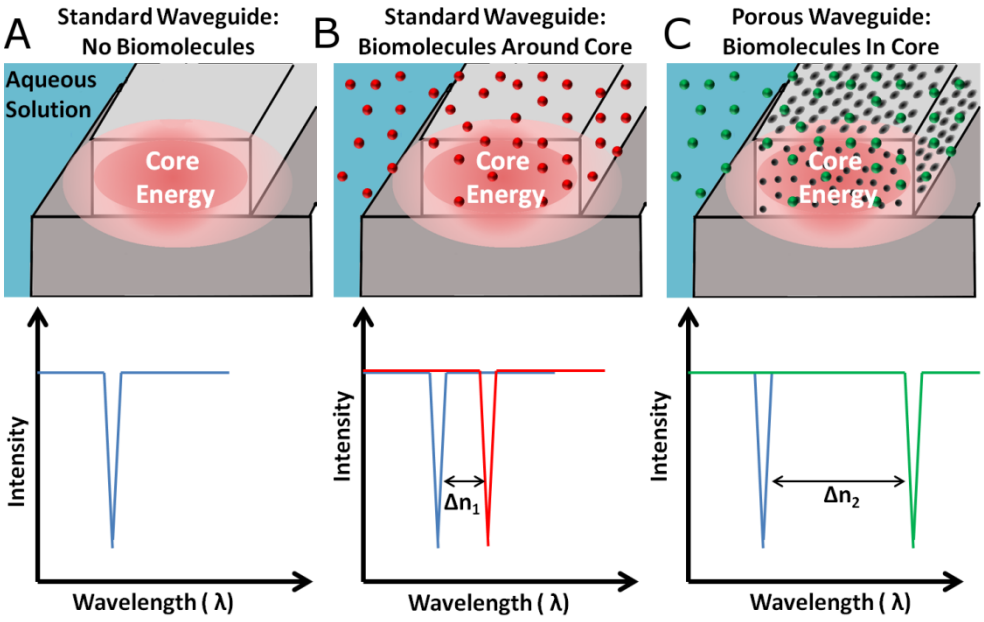

Fig. 1 (a) Traditional on chip optical biosensors rely on biomolecules interacting with a traveling waves evanescent field instead of the much higher core energy. (b) When biomolecules are present, the optical path length increases and the resonance of a ring resonator red shifts. (c) Here we demonstrate polymer devices where biomolecules more strongly interact with the core electromagnetic energy by directly entering pores in the resonator. Because of increased interaction with the electromagnetic energy, the resonance peak shifts further (Δn2 > Δn1).

In this paper, we present a method of increasing the sensitivity of optically resonant polymer biosensors. Ring resonators are chosen for their relatively high Q factors and excellent ability to localize optical energy. By creating porous resonators, bioanalytes in the detection medium are enabled to interact with the core waveguide energy increasing the effect these molecules have on the devices resonance, and thus increasing the devices sensitivity, as illustrated in Figure 1. The increase in sensitivity associated with added porosity stems from both an increase in the amount of bioanalyte allowed to interact with the modal energy as well as an increase in the average modal energy the bioanalytes can interact with. Together these effects allow for greater enhancements to sensitivity than a similar increase in surface area would if unaccompanied by the deeper access pores provide.

Figure 2 shows an example of a nanoporous polymer optofluidic device consisting of a ring resonator coupled to a bus waveguide. These devices are fabricated using imprint lithography, a unique blend of polymers, and a selective solvent. By using nanoporous materials, we are able to detect biomolecular interactions occurring throughout the core of the ring resonator, enabling a 40% increase in sensitivity. We demonstrate this technique using polystyrene nanoporous waveguides, which we combine with polymeric microfluidics to yield an optofluidic biosensor constructed of inexpensive polymers.

2. Methods

Figure 3 shows a schematic representation of the fabrication process. As detailed below, an imprint master was prepared using traditional photolithography and coated with an antistiction layer before embossing. Selected solvation was used to remove one polymer from a two-polymer

system, and microfluidic channels were attached to the resonators to allow localization of target biomolecules. Optical excitation studies were then performed to determine changes in the resonance and sensitivity of devices as a function of added porosity.

2.1 Mode calculations and simulations

Lumerical FDTD software (Lumerical Solutions, Inc, Vancouver, British Columbia, Canada) was used to analyze mode profiles and ring resonators in order to determine the effective refractive indices of our waveguides as well as approximate resonator characteristics. Three dimensional calculations of mode profiles produced effective refractive indices for our waveguides which were then used to determine optimal waveguide cross-sections as well as approximate ring radii and coupling lengths.

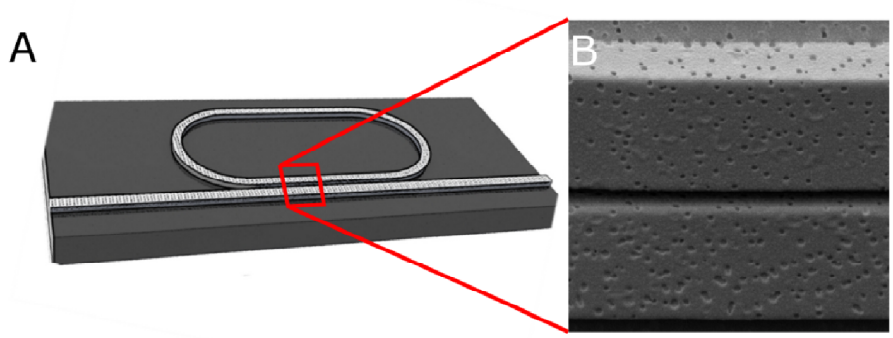

Fig. 2. (a) An illustration of porous waveguides and a ring resonator show the underlying device structure. A ring resonator was chosen in order to increase sensitivity by further localizing light to a porous location. (b) A scanning electron micrograph (SEM) of two adjacent porous waveguides highlights how interactions can occur both around and in the waveguide core.

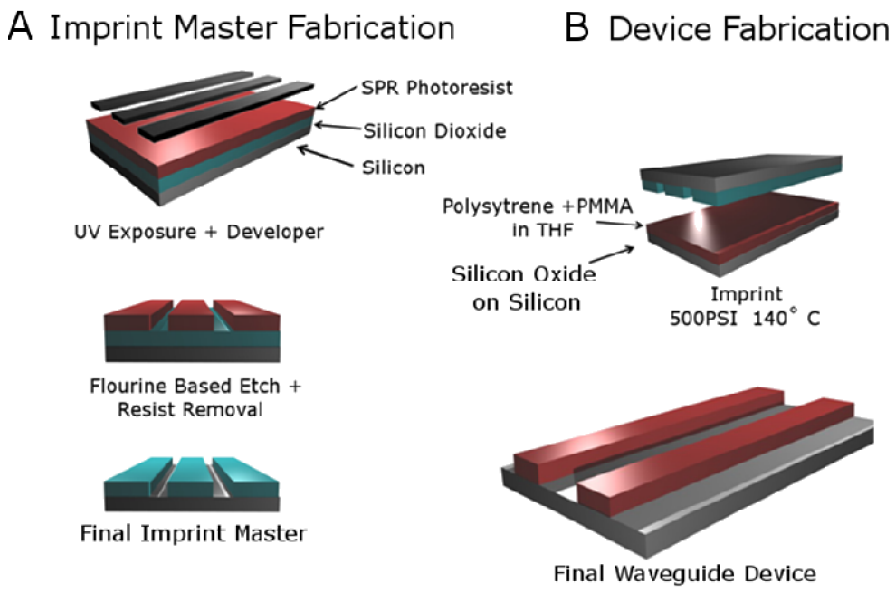

Fig. 3. A two step lithographic process was employed to create nanoporous waveguides. (a) First, an embossing master was created out of silicon oxide using standard photolithographic techniques and fluorine based etching. (b) Second, a custom polymer resist was spun onto a silicon oxide on silicon wafer, imprinted using the embossing master, and then developed using a select solvent.

2.2 Silicon master preparation

Hot embossing masters were fabricated from silicon wafers. A 2 µm film of undoped silicon oxide was deposited onto clean silicon wafers using plasma enhanced chemical vapor deposition. Wafers were then treated with P10 primer for ten seconds to promote photoresist adhesion, after which SPR 955 - 0.9 (MicroChem Corporation, Newton, MA, USA) positive photoresist was spun at 3000 rpm for 30 seconds. After a 90 second soft bake at 90 ^{o}C, wafers were patterned on an i-line autostepper, subjected to a post exposure bake of 90 seconds at 115 ^{o}C, and developed for one minute in AZ300-MIF alkaline developer. Patterned wafers were anisotropically etched

on an Oxford PlasmaLab 80+ using fluorine based gas chemistry (50 sccm CHF_3, 2 sccm O_2, 50 mTorr, 200 W) to yield 1.1 µm deep features. After stripping residual photoresist, etched masters were cleaned for 10 minutes with oxygen plasma. This cleaning process was used to ensure uniformity and stability of the anti-stiction coating ((1H,1H,2H,2H-perfluorooctyl)trichlorosilane, FOTS) which was deposited using molecular vapor deposition in order to prevent stiction between the silicon master and the polymer substrate during imprint.

2.3 Substrate preparation

A 3 µm film of undoped silicon oxide was vapor deposited onto clean silicon wafers to serve as a lower cladding material beneath the polymer waveguides and ring resonators. An 80:20 weight ratio blend of polystyrene (PS, M_w 13,502, Pressure Chemical Company, Pittsburgh, PA, USA) and polymethylmethacrylate (PMMA, M_w 15,000, Scientific Polymer Products, Ontario, NY, USA) was dissolved to 5% by weight in tetrahydrofuran. After filtering through a 0.22 µm nylon syringe filter, the polymer blend was spun on wafers for 30 seconds at 2000 rpm, followed by curing at 145 ^oC for five minutes to drive off residual solvent.

2.4 Hot embossing

Polymer waveguides and ring resonators were formed using nanoimprint lithography (Nanonex, Monmouth Junction, NJ, USA). Polymer substrates were brought into contact with silicon masters and degassed for 2 minutes during the chamber pump down. Substrates and masters were heated to 130 ^oC and pressurized to 120 psi to precondition the polymer, followed by

embossing at 140 ^{o}C and 500 psi for four minutes. In agreement with the previous literature, because of the aspect ratio between the waveguide structures and the thin polymer film, for many patterns higher pressure was needed than when imprinting other features [12-13]. Substrates were cleaved by marking the edge of the wafer onto which the polymer waveguides had been embossed using a diamond scribe, and carefully snapping the wafer along one of its crystal planes. Scanning electron microscopy revealed that this technique yielded smooth polymeric end facets, free of debris or roughness (see Figure 5b). On average this technique allowed us to yield approximately six working devices from a four inch wafer imprinted with a total of nine devices.

2.5 Nanopore development

Nanopores were introduced to the embossed optical structures by selectively developing out PMMA from the PMMA-PS composite devices. Ring resonators were covered in a droplet of dimethylsulfoxide (DMSO) for 2 hours, followed by rinsing in water and drying under filtered air. Because of the different solubility characteristics of PS and PMMA in DMSO only PMMA is removed this way leaving a porous polystyrene waveguide behind. Further, by localizing pores to only the resonators, and not the entire bus waveguide, transmission loses were significantly reduced. If pores were created by placing the devices in bulk DMSO solutions, pores developed much faster (2-10minutes), likely attributed to the better mass transport of the larger solvent. For longer times in DMSO the waveguide structures delaminate from the underlying silicon oxide. Additionally, development based on oxygen plasma was also investigated. By etching devices in oxygen plasma for 3 to 5 minutes PMMA can be removed from PS due to its higher reactivity with the oxygen species.

2.6 Surface analysis

The morphology of nanoporous waveguides and resonators, as well as the integrity of embossed structures, were observed using scanning electron microscopy. A thin gold layer (<5 nm) was sputtered onto the waveguide structures prior to imaging and scanning electron microscopy was performed at energies between 1keV and 2 keV. Refractive indices of the polymers were determined on a Woollam Spectroscopic Ellipsometer scanning at angles of incidence ranging from 65^{o} to 75^{o}, varying wavelength from 3,000 to 10,000 Å. Film thickness was characterized using a FilMetrics Optical Film Measurement System (Filmetrics, Inc., San Diego, CA). Freeze fracture techniques in liquid nitrogen were also employed in order to determine the extent and depth of porosity.

2.7 Microfluidic channels

Microfluidic masters were fabricated using standard photolithography techniques and SU-8. Poly (dimethylsiloxane) (PDMS, Ellsworth Adhesives) molds were produced using soft lithography and aligned to our optical chips using a set of translational stages and a microscope. Holders for the device were laser cut out of Plexiglas and fit around the fluidic and optical layers as shown in Figure 4. This technique was used over traditional PDMS-glass oxygen plasma bonding because of the effect oxygen plasma has on our composite material. Holes punched through the PDMS layer were fit with small metal interconnects and tubes were attached allowing flow to be induced both with a syringe manually or with a syringe pump for regulated flow velocities.

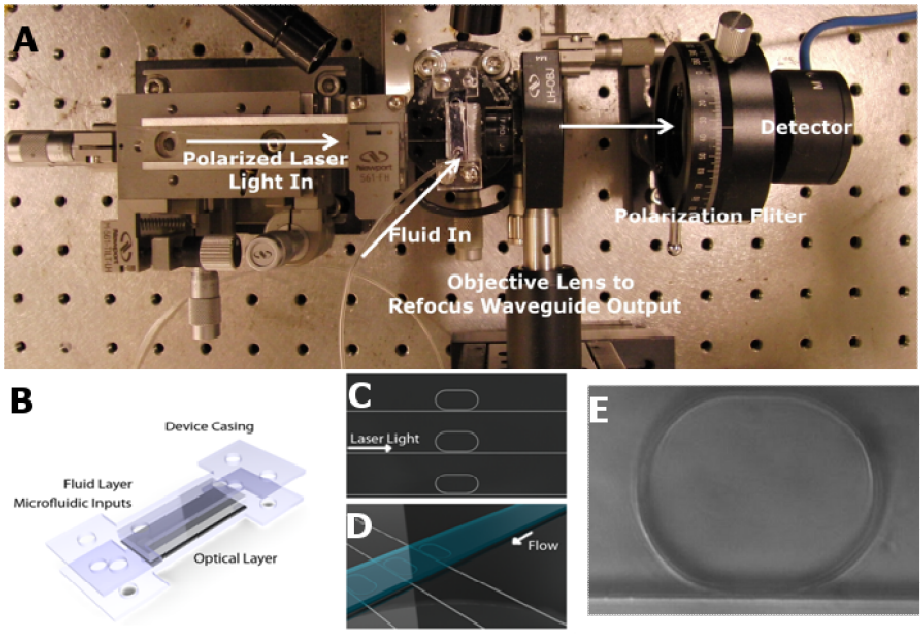

Fig. 4. (a) An illustration of the experimental setup is shown. Polarized laser light is sent through a lensed fiber and coupled into the waveguide. The waveguide is offset by 3mm to prohibit scattered light from reaching the detector and outcoming light is refocused through an objective lens, put through a polarization filter, and then reaches a photodetector. (b) Optical and microfluidic devices are shown aligned and sandwiched between two Plexiglas device holders. The final assembly is screwed closed forming a tight seal around our microfluidic channels. Illustrations show the concentration of the light (c) and fluid (d) are localized to one small area over the resonator. (e) Shows a ring resonator imaged through the device and covered in aqueous solution.

2.8 Optical excitation

An Ando AQ4321D laser source (tunable between 1520 and 1620 nm) was used to couple light into polymeric waveguides as in previous work by our group [5]. Both the fiber and the chip are

mounted on 3-axis stages to ensure accurate alignment. The input and output facets of the waveguide are shifted by 3 mm to prevent detection of scattered light. Light that passes through the waveguide is collected and collimated, then passed through a polarizer to select only the TM mode, before reaching the photodetector, as shown in Figure 4a.

2.9 Sensitivity measurements

Resonator sensitivity was determined by immersing the waveguides in an aqueous cladding solution of varying amounts of glucose. Solution refractive indices were determined using a refractometer. Glucose concentrations were chosen in order to make sure resonant peak shift from one solution to another didn't exceed the free spectral range of the devices in order to make sure peaks could be identified. Specifically, five glucose solutions were chosen at approximately 0, 5, 10, 15, and 20% to satisfy this requirement and because of availability. Solutions were measured before each experiment to confirm their refractive index.

3. Results and Discussion

3.1 Lumerical FDTD simulations

The results of our FDTD simulations indicate that polystyrene waveguides with dimensions 1 µm in height by 2.5 µm in width support both one TE and one TM mode. Because of limitations from the fabrication techniques used we were only able to place our resonators within 250 to 400 nm of the bus waveguide that evanescently coupled into them. At this spacing, our simulations

determined that the racetrack resonators would achieve the highest energy storage with a coupling length of around 20 to 30 µm. Comparing both scattering and bending losses we were able to determine that radii less than 20 µm had prohibitively high bending loses and that increases beyond radii of approximately 60 µm only seemed to increasing scattering losses. This information was used to guide the fabrication of the resonators with the goal of obtaining reasonable Q factors.

3.2 Porous resonator fabrication

Resonators were place between 250 and 400 nm from our waveguide, the closest we were able to achieve with the i-line stepper we used. We produced racetrack resonators of sizes ranging from 35 µm radii and 20 µm coupling lengths to 65 µm radii and 30 µm coupling lengths. By tuning parameters such as the ratio of the two polymers we were able to observe differences in resulting pore sizes. DMSO selectively removed PMMA from polystyrene without adversely affecting the polystyrene waveguide structure (Figure 5). Additionally, oxygen plasma etching created even more porous structures, but was difficult to isolate to only the ring region resulting in devices which scattered too much to optically excite and measure (Figure 6). Using a cleave and snap technique we were able to repeatedly generate smooth edges for light coupling with no deformation or debris. Porosity in solvent generated waveguides and resonators was approximately 9-10% of their surface area with pore diameters on the order of 60 to 120 nm and depths on the order of a few hundred nanometers. In general, there was little interconnectedness between pores in these waveguides. Because polystyrene has a contact angle less than 90˚ [24], we suspect the pores are wetting, and that aqueous solutions are capable of penetrating into the structure.

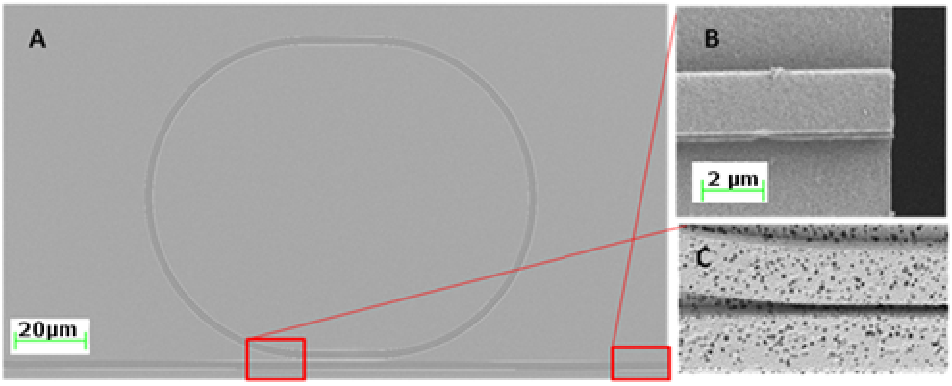

Fig. 5. (a) A scanning electron micrograph shows the complete ring resonator and its relative dimensions. (b) The end facets generated by our cleave and snap technique show how precisely the waveguides can be fractured.(c) An SEM illustrates the smallest feature size on our devices and show how the ring and bus waveguide smoothly come to within a few hundred nanometers of each other. Further, pores developed with DMSO are also shown here.

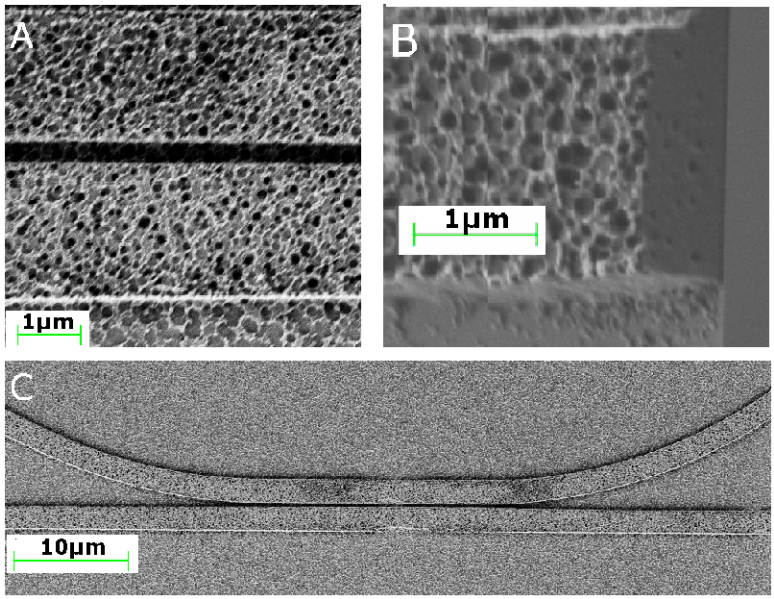

Fig. 6. (a.) A scanning electron micrograph shows a ring resonator made porous using oxygen plasma. (b) An end facet which was freeze fractured shows pores running throughout the waveguide structure. (c) A racetrack resonator and waveguide are shown separated by approximately 300 nm, the smallest top down fabricated feature on the device.

3.3 Optical excitation and resonance measurements

A typical spectrum from the resonators is shown in Figure 7. The cladding liquid here is water and approximately 1mW of laser power is coupled into the waveguide. After loses from coupling and scattering approximately 40-100 microwatts of power are collected at the detector. Depending on the exact fabrication of the resonator and any defects in it, we observed extinctions between 3 and 15dB at the resonant wavelength and Q-factors between 1000-3000. In general, we observed resonators with larger radii tended to outperform smaller ones, a factor we attributed to high bending losses due to the relatively small index difference between polystyrene and water. Resonance peaks were fit with Lorentzian functions in order to determine their location and full width half max.

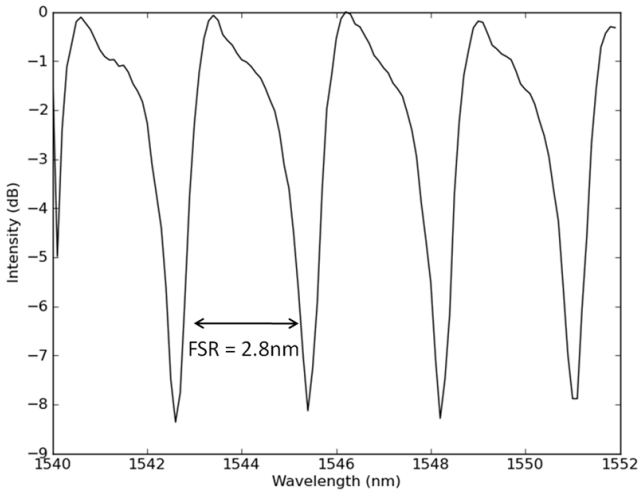

Fig. 7. A typical output spectrum of a porous resonator is shown. The free spectral range of the devices is approximately 2.8 nm, the quality factors range from 1000-3000, and on resonance wavelengths have extinctions between 3 and 15 dB.

3.4 Resonance shift as a function of porosity

As DMSO is allowed to dissolve PMMA out from our waveguide we observe a blue shift in resonance corresponding to this loss of material. Using this type of measurement we can observe pores being added to our material simply through measurements of the optical resonance of the devices. Figure 8 shows measurements taken as a device was exposed to DMSO. After each exposure to DMSO the resonators were rinsed with water and dry air before the next measurement was taken. These rinsing and drying steps are important because the refractive index of DMSO is approximately 1.48, and when the porous resonator is covered with and filled by DMSO the resonant peaks red shift. As the DMSO evaporates the resonant peaks blue shift back and reach a final stable point once the DMSO is no longer present.

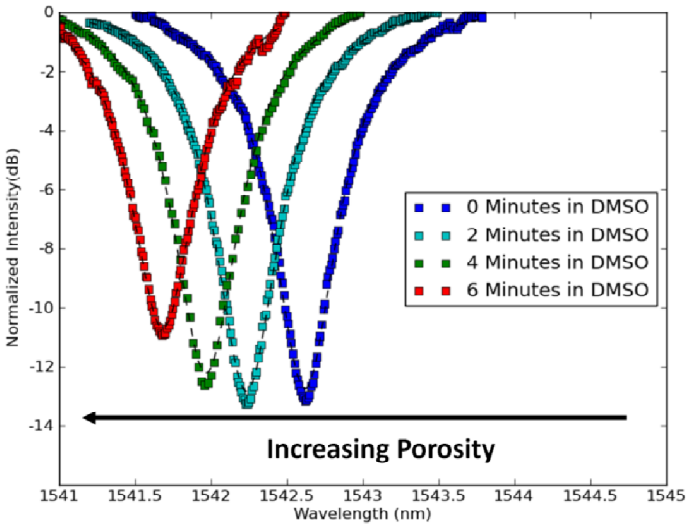

Fig. 8. As the porosity of a ring resonator increases its resonance blue shifts. This change corresponds with decreasing mass and a shorter optical path and is a good indicator that pores are being generated. Measurements of resonance were taken with the resonator immersed in water at all four time points, and conditions were controlled so the only change was the addition of pores.

3.5 Effect of porosity on sensitivity

Figure 9 shows resonances both before pores were added and after in a single device as well as SEMs of a nonporous device and after pores are added. A resonant peak is plotted at five different glucose concentrations for each resonator. Note that as the index of the cladding solution increases the resonant condition red-shifts, which corresponds with the longer optical path. This result agrees with Figure 8, where a blue-shift was observed due to a shortening of the optical path associated with the addition of pores. Due to increased interaction between the aqueous sample solution and the waveguide's core energy the change in resonance is greater in the porous device. Additionally, Figure 10 compares the sensitivity of nonporous and porous resonators, showing a 42% increase in resonator sensitivity. Standard error is used to show inter device variability, which is significantly higher for the porous resonators compared to the nonporous, a characteristic we attribute to different porosity arising during fabrication. Both sets of data were fit with a linear regression running through the origin and sensitivities of 66.15 and 94.05 were determined. The nonporous and porous resonator sensitivities have coefficient of determination (R^2) values of .995 and .968, respectively, both indicating a good fit.

4. Conclusions

In this work we have shown how porous polymer waveguides can be fabricated using nanoimprint lithography and selective solvents. The porous structures created provide higher sensitivity than their nonporous counterparts and the modification can be performed in only one additional step using only a solvent. This modification can be made prior to functionalization and fits naturally into the creation of ring resonator biosensors. Additionally other changes could be made to further enhance the sensitivity of porous waveguides. One example is the use of wetting

agents that could allow bioanalytes to penetrate deeper into the porous waveguide structure and further increase sensitivity. A second example involves allowing bioanalyte solution to dissolve on the waveguide, concentrating the molecules of interest into the pores, where they would be capable of causing a greater change in sensitivity. One limitation in this work is the lack of quantitative biomolecular sensing studies. In future work we plan on functionalizing these porous waveguides for certain biomarkers and determining how their porous nature effects these detection reactions.

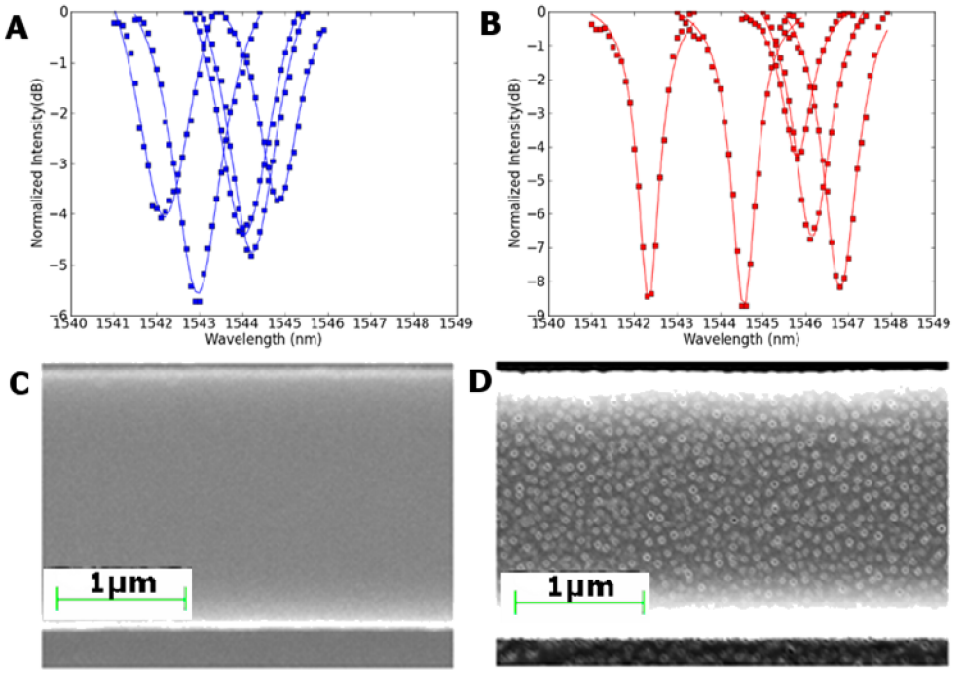

Fig. 9. The resonance shift of nonporous (a) polymer resonators is compared to their (b) porous counterparts. Measurements are taken at five different concentrations of glucose between 0 and 20 percent. As the refractive index of the cladding solution increases, a corresponding red shift is seen in the resonance condition of the rings. Because of increased bioanalyte electromagnetic energy interactions occurring in the porous waveguide the sensitivity of the device is significantly increased, and further shifts can be observed in (b) than (a). SEMs of a waveguide without pores (c) and of the waveguide after pores (d) are added are also shown.

The work presented here only shows a simple application of how two-polymer systems can be used to create interesting nanostructures for optics. Here the polymers are mixed in suspension and allowed to phase separate into random arrangements. In theory, it's possible to imagine that by creating diblock copolymers or other similar systems that two polymers could be caused to assemble into long-range ordered structures [25]. These nanostructures could not only allow for increased sensitivity in ring structures but could also potentially be used to create interesting optical materials, including self-assembled photonic crystals.

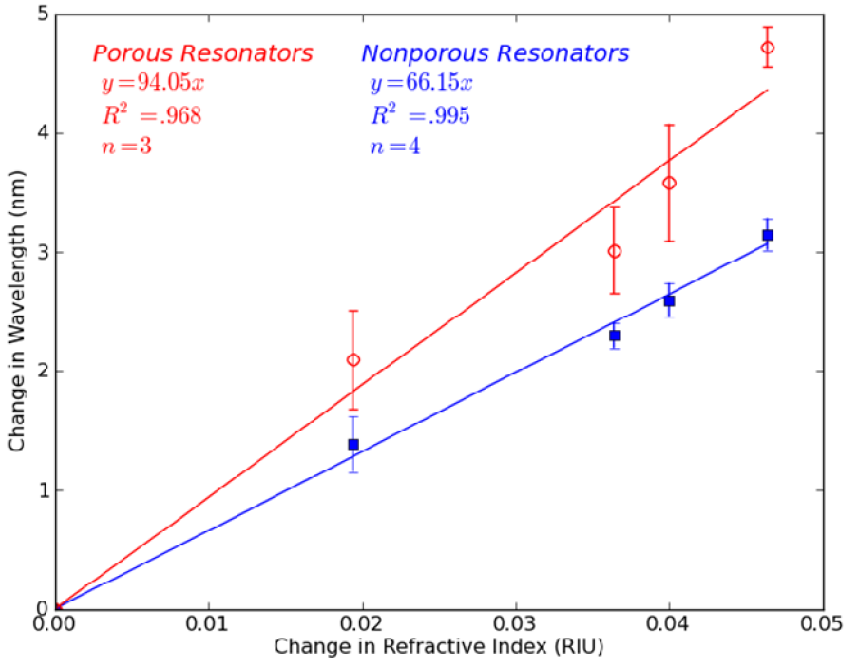

Fig. 10. The sensitivity of a porous resonator is plotted against that of a nonporous resonator. An increase in over 40% sensitivity can be seen. The first data point appears at 0 corresponding to the resonator immersed in water.

We have shown that by using simple polymer techniques the sensitivity of optical resonators can be increased by over 40%. While the sensitivity of polymer devices is generally lower than

traditional silicon devices these porous additions can provide polymer ring resonators an advantage. This increase in sensitivity combined with the simple fabrication and low cost associated with polymers can provide a distinct advantage to these devices and a simple way to make highly sensitive inexpensive biosensors.

5. Acknowledgements

This material is based upon work supported by the National Science Foundation Graduate Research Fellowship under Grant No. DGE-0707428. Additional support for this work was provided by the National Institutes of Health - National Institute of Biomedical Imaging and Bioengineering (NIH-NIBIB) under grant number R21EB007031. This work made use of STC shared experimental facilities supported by the National Science Foundation under Agreement No. ECS-9876771. The authors gratefully acknowledge Michael Mak for assistance in mode calculations, Sudeep Mandal for assistance in light coupling experiments, Xavier Serey for help with resonator simulations, and all three for numerous technical discussions.

6. References

1. Cooper, M.A., *Label-free screening of bio-molecular interactions.* Analytical and Bioanalytical Chemistry, 2003. **377**(5): p. 834-842.
2. Erickson, D., et al., *Nanobiosensors: optofluidic, electrical and mechanical approaches to biomolecular detection at the nanoscale.* Microfluidics and Nanofluidics, 2008. **4**(1-2): p. 33-52.

3. Anker, J.N., et al., *Biosensing with plasmonic nanosensors.* Nature Materials, 2008. **7**(6): p. 442-453.

4. Vollmer, F. and S. Arnold, *Whispering-gallery-mode biosensing: label-free detection down to single molecules.* Nature Methods, 2008. **5**(7): p. 591-596.

5. Mandal, S. and D. Erickson, *Nanoscale Optofluidic Sensor Arrays.* Optics Express, 2008. **16**(3): p. 1623-1631.

6. Daniels, J.S. and N. Pourmand, *Label-free impedance biosensors: Opportunities and challenges.* Electroanalysis, 2007. **19**(12): p. 1239-1257.

7. Lange, K., B.E. Rapp, and M. Rapp, *Surface acoustic wave biosensors: a review.* Analytical and Bioanalytical Chemistry, 2008. **391**(5): p. 1509-1519.

8. Yariv, A., *Universal relations for coupling of optical power between microresonators and dielectric waveguides.* Electronics Letters, 2000. **36**(4): p. 321-322.

9. Yariv, A., *Critical coupling and its control in optical waveguide-ring resonator systems.* Ieee Photonics Technology Letters, 2002. **14**(4): p. 483-485.

10. Seo, B.J., et al., *Design of ring resonators using electro-optic polymer waveguides.* Journal of Physical Chemistry C, 2008. **112**(21): p. 7953-7958.

11. Xu, D.X., et al., *Folded cavity SOI microring sensors for high sensitivity and real time measurement of biomolecular binding.* Optics Express, 2008. **16**(19): p. 15137-15148.

12. Chao, C.Y. and L.J. Guo, *Polymer microring resonators fabricated by nanoimprint technique.* Journal of Vacuum Science & Technology B, 2002. **20**(6): p. 2862-2866.

13. Chao, C.Y., W. Fung, and L.J. Guo, *Polymer microring resonators for biochemical sensing applications.* IEEE Journal of Selected Topics in Quantum Electronics, 2006. **12**(1): p. 134-142.

14. Mandal, S., J.M. Goddard, and D. Erickson, *A multiplexed optofluidic biomolecular sensor for low mass detection.* Lab on a Chip, 2009(DOI: 10.1039/b907826f).

15. Martin, A.L., et al., *Replica-molded high-Q polymer microresonators.* Optics Letters, 2004. **29**(6): p. 533-535.

16. Myers, F.B. and L.P. Lee, *Innovations in optical microfluidic technologies for point-of-care diagnostics.* Lab on a Chip, 2008. **8**(12): p. 2015-2031.

17. De Vos, K., et al., *SOI optical microring resonator with poly(ethylene glycol) polymer brush for label-free biosensor applications.* Biosensors & Bioelectronics, 2009. **24**(8): p. 2528-2533.

18. Barrios, C.A., *Optical Slot-Waveguide Based Biochemical Sensors.* Sensors, 2009. **9**(6): p. 4751-4765.

19. Barrios, C.A., et al., *Slot-waveguide biochemical sensor.* Opt. Lett., 2007. **32**(21): p. 3080-3082.

20. Rabus, D.G., et al., *A bio-fluidic-photonic platform based on deep UV modification of polymers.* IEEE Journal of Selected Topics in Quantum Electronics, 2007. **13**(2): p. 214-222.

21. Kehagias, N., et al., *Embedded polymer waveguides: design and fabrication approaches.* Superlattices and Microstructures, 2004. **36**(1-3): p. 201-210.

22. Xu, F., et al., *Polymer microfluidic chips with integrated waveguides for reading microarrays.* Analytical Chemistry, 2007. **79**(23): p. 9007-9013.

23. Goddard, J.M. and J.H. Hotchkiss, *Polymer surface modification for the attachment of bioactive compounds.* Progress in Polymer Science, 2007. **32**(7): p. 698-725.

24. Li, Y., et al., *Contact Angle of Water on Polystyrene Thin Films: Effects of CO2*

Environment and Film Thickness. Langmuir, 2007. **23**(19): p. 9785-9793.

25. Mahajan, S., et al., *Synthesis and Characterization of Amphiphilic Poly(ethylene oxide)-block-poly(hexyl methacrylate) Copolymers.* Macromolecular Chemistry and Physics, 2003. **204**(8): p. 1047-1055.

CHAPTER 3

MULTIPLEXED COLORIMETRIC DETECTION OF KAPOSI'S SARCOMA ASSOCIATED HERPESVIRUS AND BARTONELLA DNA USING GOLD AND SILVER NANOPARTICLES

Kaposi's sarcoma (KS) is an infectious cancer occurring most commonly in human immunodeficiency virus (HIV) positive patients and in endemic regions, such as Sub-Saharan Africa, where KS is among the top four most prevalent cancers. The cause of KS is the Kaposi's sarcoma-associated herpesvirus (KSHV, also called HHV-8), an oncogenic herpesvirus that while routinely diagnosed in developed nations, provides challenges to developing world medical providers and point-of-care detection. A major challenge in the diagnosis of KS is the existence of a number of other diseases with similar clinical presentation and histopathological features, requiring the detection of KSHV in a biopsy sample. In this work we develop an answer to this challenge by creating a multiplexed one-pot detection system for KSHV DNA and DNA from a frequently confounding disease, bacillary angiomatosis. Gold and silver nanoparticle aggregation reactions are tuned for each target and a multi-color change system is developed capable of detecting both targets down to levels between 1 nM and 2 nM. The system developed here could later be integrated with microfluidic sample processing to create a final device capable of solving the two major challenges in point-of-care KS detection.

Mancuso, M., Jiang, L., Cesarman, E., Erickson, D. "Multiplexed Colorimetric Detection of Kaposi's Sarcoma Associated Herpesvirus and Bartonella DNA using Gold and Silver Nanoparticles" *Nanoscale* 5, 1678-1686 (2013)

1. Introduction

With the onset of the acquired immunodeficiency syndrome (AIDS) epidemic in the early 1980s, one of the first indicators of infected patients was the presence of red skin lesions, a symptom of a disease known as Kaposi's sarcoma (KS) [1-4]. Before the discovery of the cause of AIDS, KS and other opportunistic infections were often the first signs, and biggest complications, for infected individuals. During this time significant research efforts were made to determine the cause of AIDS, and in 1983 HIV was discovered [5-6]. A little over ten years later the cause of KS was first connected to a second virus, Kaposi's sarcoma-associated herpesvirus (KSHV), later given the alternative designation of human herpesvirus 8 (HHV-8) [7].

Today, KS is still the most prevalent cancer in untreated HIV-infected individuals. Initial studies showed that it affected 1 in 20 HIV-positive patients [8]. With the introduction of highly active anti-retroviral therapy (HAART), patients in the developed world have seen improvements in the management and treatment of KS, but it remains increased in incidence as compared to the pre-AIDS era in HIV-infected patients [9-10]. In regions of the developing world, such as Sub-Saharan Africa, both HIV and KS are endemic, and KS is the fourth leading cancer in the region [11]. In some countries such as Uganda, KS is the number one cause of cancer in men [11-12].

The infectious cause of KS is now well known to be the oncogenic herpesvirus KSHV or HHV-8 [7, 13]. While the details of transmission are still being studied, it is most likely through saliva [14-16] and in some regions KSHV rapidly spreads beginning in childhood affecting large portions of the population, reaching seroprevalence of over 50% [11,17]. Like other herpesviruses, KSHV can establish a latent infection, and remains without causing any disease for the remaining life in most infected hosts, being necessary but not sufficient of KS

development. In locations where the seroprevalence of KSHV is this high, the clinically relevant test becomes determining if KSHV is present in a specific tumor, and not simply if it is present in a person's blood.

A second issue arises because of a number of other diseases have a similar presentation as Kaposi's sarcoma, and are part of the differential diagnosis [18-20]. KS most often presents as a collection of red lesions, and when looked at on a typical hematoxylin and eosin (H&E) stained histology slide has a number of unique features, including vascular spaces and proliferation of spindle cells thought to be of lymphatic endothelial origin [13, 21]. However, while these features are characteristic of KS, a number of other diseases, including bacillary angiomatosis (BA) caused by Bartonella henselae or quintana, and pyogenic granuloma with no known infectious cause, can often have a similar clinical and histological appearance and represent a diagnostic challenge [18-19].

In developed clinical settings, skin biopsies are easily processed for histology using advanced tools including tissue processing systems and microtomes. KS diagnosis can then be made after an H&E staining through microscopic evaluation by a pathologist, and when the histological characteristics are uncertain, the presence of KSHV is determined to confirm the diagnosis either with immunohistochemistry specific for unique KSHV proteins or polymerase chain reaction (PCR) specific for unique KSHV DNA sequences. While the professional expertise and methods for sample preparation and diagnostic techniques are available in developed nations, they are scarce or nonexistent in many of the places where KS is most prevalent. If affordable point-of-care diagnostics could be created that are capable of distinguishing KS from other similar conditions, better treatment could be provided.

Ultimately, two unique challenges present themselves in the creation of point-of-care diagnostics for Kaposi's sarcoma in the developing world. The first is the requirement for the detection of KSHV in a biopsy sample without reliance on common laboratory technology. Extracting DNA from a skin biopsy sample using only simple, robust technology has thus far received little attention. The second challenge involves the presence of other diseases that can mimic KS, and thus the need for creating multiplexed detections that can distinguish one from the other. Further, these multiplexed detection systems need to be easily integrated to work with a small sample size, and in the presence of whatever surfactants and contamination is left over after DNA extraction.

While diagnostics in the developing world in general pose a number of challenges, a large amount of work has been done addressing them. Recently an abundance of biosensors have been developing using mechanical [22-23], electrical [24], and optical [25], techniques to detect bioanalytes in minute quantities. Many of these devices combine microfluidics and other nanotechnologies in order to create tools which both operate at the length scale of the detection target and at a macroscopic scale which can be simply read-out. A number of them have even been applied in the developing world, where the additional constraints placed on devices by a lack of resources and trained personnel compound issues further [26-27]. Yet for all of the successes of these biosensors, a number of limitations still exist, including the need to pre-process samples, the ability to work in a range of buffers (including those used to lyse cells), high sensitivity limits, and often a limited ability to detect multiple targets.

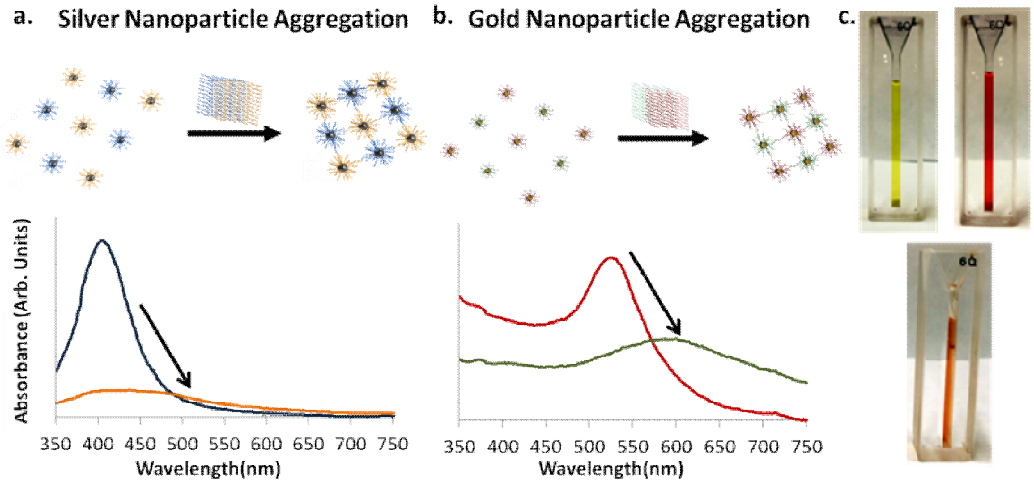

Fig. 1(a) and (b) Illustrate the aggregation of silver and gold nanoparticles in the presence of target DNA. As the nanoparticles aggregate their surface plasmons couple, the resonance condition changes, and their characteristic optical peaks red shift. (c) 600uL of gold nanoparticles, silver nanoparticles and a combination of both are shown, illustrating their optical properties. In the orange gold and silver solution each type of nanoparticle can be functionalized to react differently, allowing for either color change reaction to take place independently.

Perhaps some of the most interesting recently developed diagnostic technologies are those which link the presence of a bioanalyte to changes in the localized surface plasmon resonance of metal nanostructures [28-30]. These devices are both highly sensitive and produce a convincing color-change that is discernible to the naked eye. To date techniques using nanoparticle based detection schemes have been applied to the recognition of oligonucleotides [31-32], proteins [33], metal ions [34], and other small molecules [35-36]. In the form of metal nanoparticles, localized surface plasmon resonance biosensors often rely on some target molecule to trigger particle aggregation. When nanoparticles aggregate as illustrated in Figures 1a and 1b, the

particles surface plasmons couple and their resonance condition changes. These colorimetric detection reactions were initially developed with sensitivities around 1nM to 10nM [31, 37]. Later work examined the limitations of these colorimetric nanoparticle aggregation detections, and determined the detection limit is ultimately a function of the relative concentration of nanoparticles to the concentration of DNA, and the size and optical cross section of the nanoparticles (among a few other factors) [28]. By using larger nanoparticles (~50nm) or a material with a higher optical cross section (i.e. silver) these colorimetric nanoparticle detection schemes have been optimized to reach sensitivities in the 50pM to 1nM range [28, 32, 38].

Additionally, a number of other nanoparticle based detection schemes exist, which use the same recognition reaction, but a different sensing mechanism. Examples include scanometric based detection in which gold nanoparticles bind to a surface and are then made visible through the deposition of silver on their surface [26,39], bio-barcode based detection schemes where the DNA signal is amplified before a similar silver deposition [40], and simple spot-and-read tests where light from an illuminated glass slide is evanescently coupled into gold nanoparticles after aggregation [30]. It is difficult to produce a single low limit of detection because of the number of techniques and targets which exist, but nanoparticle based colorimetric detection schemes that integrate waveguiding glass slides have been shown to go to detection limits as low as approximately 300fM [30], and bio-barcode techniques have been shown to reach as low as sub-attomolar detection limits [40-42].

Table 1 Probe and Target Sequences for KSHV and BA

Name	Sequence	T_M (°C) 300mM NaCl
KSHV Probe 1	AAAAAAAAAAAAAAAGCCAACGTCATTCCGCAGGAT	76.1
KSHV Probe 2	AAAAAAAAAAAAAAAAGGCTGTGCGCTGTTGGTTCCT	78.7
KSHV Target	ATCCTGCGGAATGACGTTGGCAGGAACCAACAGCGCACAGCCT	96.5
Bartonella Probe 1	AAAAAAAAAAAAAAACCAATCGGTGGAGACGG	70.2
Bartonella Probe 2	AAAAAAAAAAAAAAACGCTGACCAAGAGCAGGA	71.3
Bartonella Target Sequence	CCGTCTCCACCGATTGGTCCTGCTCTTGGTCAGCG	94.2

Recently, smartphone based technologies have also been combined with a number of colorimetric technologies, allowing for point-of-care detection and quantification of target levels using pre-existing technology [43-44]. One pertinent example includes the use of a gold-on-paper platform and a smartphone camera in order to detect DNA sequences from Mycobacterium tuberculosis, the cause of Tuberculosis [45].

Here we present a solution to the differential diagnosis of KS and BA based on a colorimetric one-pot gold and silver nanoparticle system (Figure 1c). By combining these two oligonucleotide detection techniques in one solution we create a sysem that has two independent color change reactions depending on the DNA target present. We present both the visible color change associated with these detection reactions as well as the changes in the solutions optical spectrum and show the limit of detection of the system approaches single nanomolar concentrations. We demonstrate that our color change reactions have similar sensitivities to other aggregation reactions (~1nM), and that the two reactions do not interfere with each other. Because this multiplexed detection scheme can be carried out in one solution, it can later easily be integrated into a microfluidic device which solves the second challenge in KS detection, working with biopsy samples. Further, additional techniques, including illumination through an evanescently coupled glass slide, could later be utilized to further enhance our limit of detection.

2. Experimental Section

2.1 Primer Design and Selection

Oligonucleotide sequences were chosen for KSHV using BLAST Primer Design [46] to determine short DNA sequences (~20 BP) for DNA that codes for vCyclin, a KSHV protein known to express itself both during the latent and lytic viral phases [47]. The fact that vCyclin is expressed both latently and lytically could later be useful, because direct detection of extracted RNA could provide an additional template for amplification. Bacillary angiomatosis, a bacterial infection, can be caused by two different species, Bartonella quintana and henselae [48], and primers were designed to be specific to both agents. Briefly, the two bacteria genomes were compared to find conserved regions, a reference genome was created out of the conserved regions, and BLAST Primer Design was used to find oligonucleotides specific to these regions. A 15 base long polyadenine sequence was added to the 5' end of the sequences, followed by an alkyl thiol group used to bind the oligonucleotides to gold particles. All oligonucleotides were ordered from Invitrogen (Grand Island, NY), and their sequence information can be found in Table 1.

2.2 Gold and Silver Nanoparticle Functionalization

Gold and silver particles with average diameters of 15 and 20 nm, respectively, were functionalized using thiol based chemistry using methods described by others [31-32, 37]. These sizes were chosen as a compromise between larger particles which generally provide higher

sensitivity [38], and smaller particles which are generally easier to make stable in salt solutions. Briefly, 50 µL of 100 µM oligonucleotides with 5' alkyl thiol groups was added to 1 mL solutions of gold (3 nM) and silver (750 pM) nanoparticles in excess and allowed to react overnight. The solution was then brought to 10mM sodium phosphate and .01% sodium dodecyl sulfate (SDS), and again given 24 hr to react. This process was repeated, this time adding sodium chloride, resulting in final concentrations of 100 mM, 200 mM, and 300 mM, each time with 24 hrs in between. These increasing molarity salt solutions are used to screen electrostatic interactions between DNA strands, ultimately allowing for a higher density layer to be formed on the surface of the nanoparticles. After the final incubation period, solutions were spun down and resuspended in .01% SDS three times to remove excess oligonucleotides, and finally brought to 10 mM Sodium Phosphate and 300 mM Sodium chloride.

2.3 Melting Temperature Analysis

In previous literature Storhoff et al. [37] and Thompson et al. [32] have shown how gold and silver nanoparticle-based aggregation can have specificity high enough to determine single nucleotide mismatches between targets. A perfect and one nucleotide mismatched target have different melting temperatures, and by measuring what temperature the nanoparticles disassociate one can distinguish between the two. A similar disassociation temperature is determined here for a correct target for both nanoparticle systems, and further detection reactions are performed at a temperature just below this threshold to insure incorrect targets don't cause any aggregation. KSHV and Bartonella DNA (10 nM) sequences were added to solutions of conjugated gold and silver nanoparticles respectively, and the solutions were allowed 4 hr to

aggregate. Then, the solutions were heated in 5 degree increments from 45 °C to 95 °C to determine at what temperature the nanoparticles disassociated.

2.4 KSHV and BA Detection and Sensitivity Measurements

Solutions of gold and silver nanoparticles were mixed to yield a final concentration of 1.5 nM gold nanoparticles and 325 pM silver nanoparticles. Due to silver's higher absorption cross section, a lower concentration was used. Target and Control DNA were added at concentrations of 5 nM and solutions were kept 2 hrs at 65 °C to react before their absorbance measurements were recorded. Similarly, experiments were conducted to measure the limit of detection of the system. Different concentrations of DNA from 10 pM to 1 uM were added to 40 µL of both silver and gold independently to measure the sensitivity of each channel. Solutions were given 2 hr at 65 °C to react, and their near UV and visible spectrums were collected.

2.5 Materials and Instrumentation

Spectrophotometric measurements were taken using a Spectramax plus 384 (Molecular Devices, Sunnyvale, CA) in the Nanobiotechnology Center at Cornell University. SEMs were taken on a Zeiss Ultra (Oberkochen, Germany) in the Cornell Center for Nanofabrication. Gold nanoparticles were purchased from Nanopartz (Loveland, CO). All other reagents were purchased from Sigma-Aldrich (St. Louis, MO).

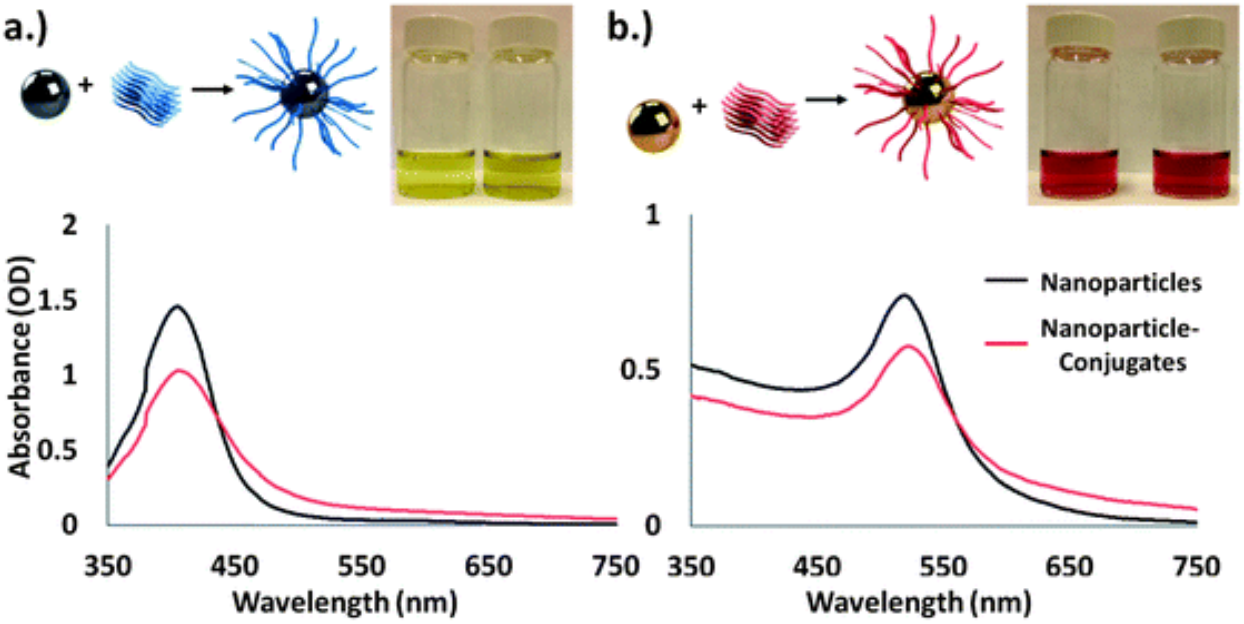

Fig. 2 (a) Silver and (b) Gold Nanoparticles functionalized using thiolated oligonucleotides. After conjugation, both spectrums red shifted by approximately 1-3 nm, as similarly reported in previous literature. The change in total absorption is mostly due to incompletely collection of the nanoparticles after conjugation. Silver and gold particles after conjugation are shown in the inset images respectively.

3. Results and Discussion

3.1 Nanoparticle-Oligonucleotide Conjugation

The attachment of oligonucleotides to gold and silver nanoparticles yielded homogenous stable solutions of nanoparticle conjugates the same color as the original solution. As in previous work by Storhoff et al. and Thompson et al., a small change of roughly 1 to 3 nm in nanoparticle resonance was observed in accordance with the nanoparticle conjugations, as shown in Figure 2 [32, 37].

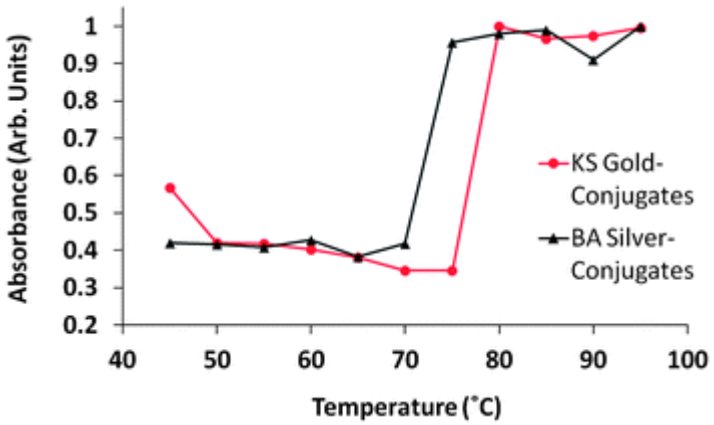

Fig. 3 After allowing solutions of the nanoparticles to aggregate the temperature that they disassociated at was determined. For both the KS and BA a sharp increase in absorbance was seen at their melting temperatures, approximately 80 and 75 degrees, respectively.

Decreases in absorbance were also observed due to incomplete collection of nanoparticles during excess oligonucleotide removal. The final gold nanoparticle solutions were stable for greater than 1 month at room temperature, while the silver particles were stable for approximately two weeks. This difference in stability is likely attributed to the different reaction constants between gold and thiol and silver and thiol.

3.2 Melting Temperature Analysis

The results of the melting temperature analysis indicated that the KSHV functionalized nanoparticles disassociated between 75 °C and 80 °C, and the Bartonella functionalized nanoparticles between 70 °C and 75 °C, as shown in Figure 3. These results line up well with the expected melting temperatures of the oligonucleotide probes, which can be found in Table 1. Further, the lower melting temperature of the Bartonella probes agrees well with the length of the

probes being 5 nucleotides shorter. These temperature results were used to choose 65 °C as the temperature that the detection and sensitivity experiments were conducted at to prevent nonspecific aggregation.

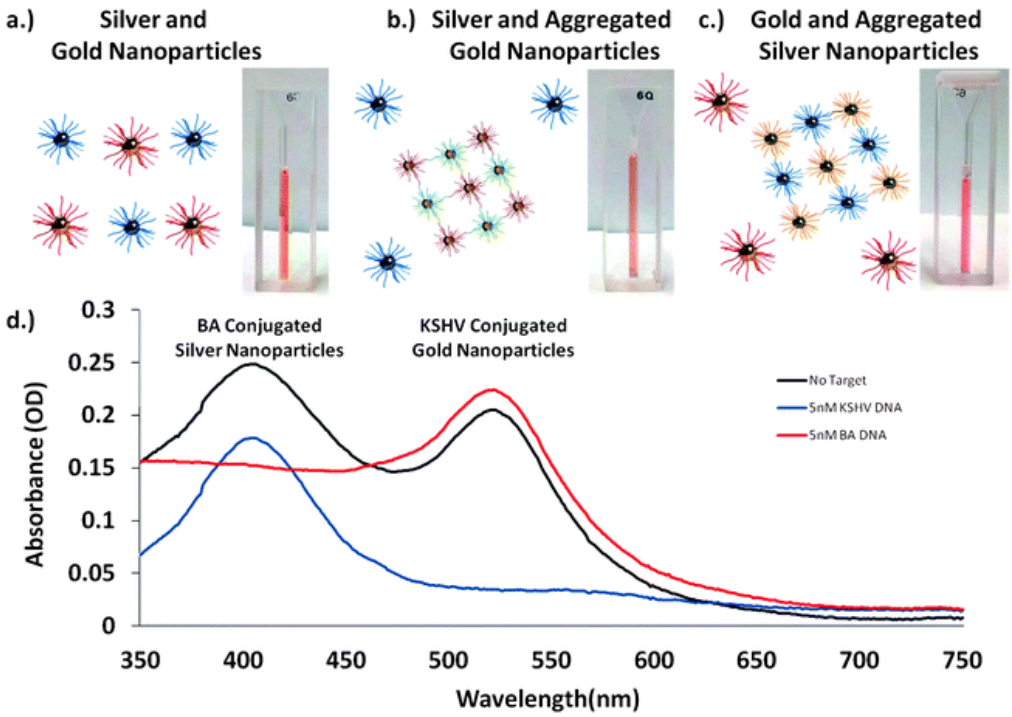

Fig. 4 (a) A solution of conjugated gold and silver nanoparticles. (b) Upon introduction of KSHV DNA the gold particles aggregate and the solution turns darker orange. (c) Upon introduction of BA DNA the silver nanoparticles aggregate, and the solution becomes bright pink. (d) An optical spectrum illustrates the change in the nanoparticles resonance as they aggregate. All DNA solutions added in these experiments were 5nM.

3.3 Multiplexed KSHV and BA DNA Detection Experiments

In experiments using both KSHV functionalized gold and Bartonella functionalized silver nanoparticles (Figure 4a), upon successful aggregation and detection of one target, the

multiplexed solution displayed a color more similar to the non-aggregated solution. For example, when Bartonella target DNA (BA DNA) was introduced to the solution the silver nanoparticles aggregated and the solution turned to a pink color, more dependent on the surface plasmon characteristics of the unaggregated gold particles (Figure 4b). When KS DNA was introduced the gold nanoparticles aggregated and the solution changed to a murky yellow-orange color, more dependent on the silver nanoparticles (Figure 4c). Spectrophotometric analysis also revealed that only the wavelength resonant peak of the nanoparticle aggregate was affected by the detection of a single target (Figure 4d). A small change in the absorption at the non-target-corresponding resonant wavelength is observed due to a change in the corresponding resonant peak's tail, but the resonant peaks wavelength did not change. Further, Scanning Electron Micrographs reveal that upon introduction of a target, an aggregation reaction does indeed occur (Figure 5). For the gold nanoparticles a color change could be visually observed as early as 30 minutes to 1 hour after addition of DNA and for the silver nanoparticles as early as one hour after the addition of target. Measuring the absorbance of the solutions we were able to see changes as soon as 10 to 20 minutes after the addition of target.

When gold nanoparticles and silver nanoparticles were mixed and stored together the silver nanoparticles would gradually and nonspecifically aggregate over the course of two to three days, even in the presence of no target. Presumably this aggregation was caused by a reaction between the thiol groups of the Bartonella probe DNA attached to the silver nanoparticles reacting with the gold nanoparticles because of thiol and gold's greater reaction constant. However, over the time span of our reactions, no change was observed in the silver nanoparticles, allowing for multiplexed detection in one solution.

3.4 Sensitivity Experiments

Detection reactions were carried out at various target DNA concentrations to determine the limit of detection of the system. Our results indicate that the limit of detection of the gold nanoparticles is approximately 2nM, and for the silver nanoparticles is approximately 1nM (Figure 6). The limit of detection of the silver nanoparticles is likely higher because their higher absorption cross section allows for a lower concentration of nanoparticles that can aggregate in the presence of less DNA. These results line up well with previous nanoparticle-based colorimetric detection, which shows limits of detection for gold around approximately 1nM, and for silver around approximately 100pM [32, 37].

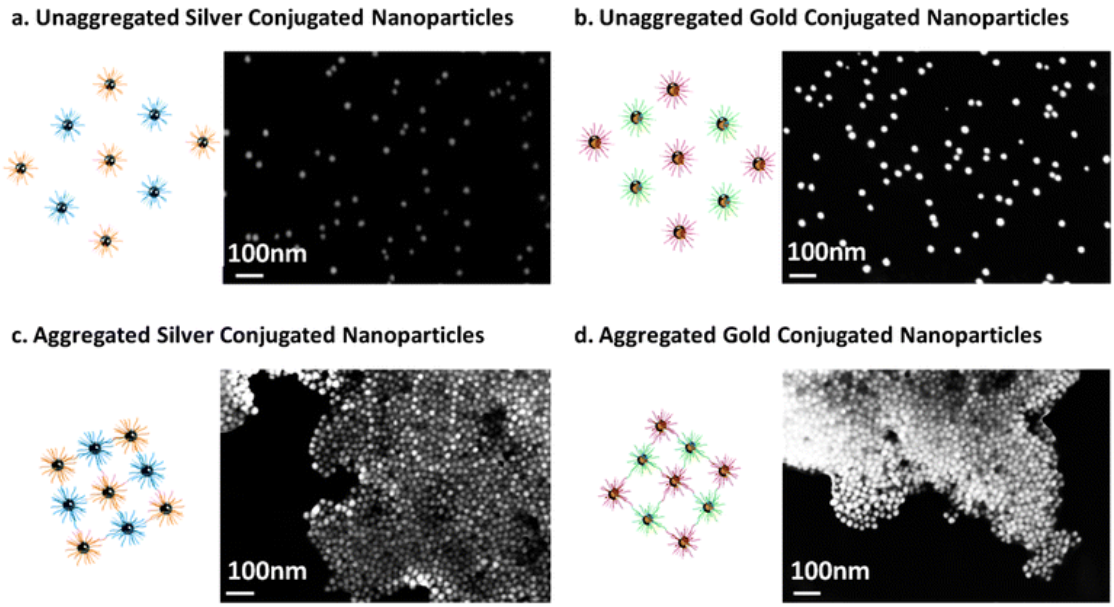

Fig. 5 Scanning electron micrographs of unaggregated oligonucleotide conjugated silver and gold nanoparticles on a silicon wafer. After the addition of target DNA the silver and gold nanoparticles form aggregates.

While these limits of detection are high for the detection of unamplified DNA, there are a number of techniques that we could later implement to allow our multiplexed system to directly detect extracted DNA. One example previously mentioned involves evanescently coupling light from illuminated glass slides into the nanoparticles to excite them as opposed to a broadband source. Storhoff et al. report a limit of detection of 300fM, demonstrating how this simple light source can provide an almost 1000 fold increase in sensitivity using the same nanoparticles [30]. Ultimately, they use their system to detect unamplified genomic DNA. A second technique which could be used to directly detect KSHVs presence involves detecting mRNA already transcribed from the genomic DNA. As explained previously vCyclin, is expressed both latently and lytically, and orders of magnitude more copies could be available for detection.

4. Conclusions

Here we have demonstrated a multiplexed colorimetric one-solution method of detecting KSHV and Bartonella DNA. We have shown that gold and silver nanoparticle conjugates can be used in one solution for colorimetric detection, and that both color change reactions can be seen independently of each other. Our results indicate that this sort of technique can be used to differentiate DNA from these two similarly presenting diseases with speeds on the same order of PCR based techniques (minutes to hours), and faster than immunohistochemistry based ones (hours to days).

In this work we demonstrate such a multiplexed detection using two targets, but it is possible to imagine that by using nanoparticles of other shapes, sizes, and materials, a multiplexed solution could be created capable of many colorimetric detection reactions for different targets.

In addition to nanospheres like those used in this work, nano- rods [49], prisms [50-51], bipyramids [52-53], and a number of other geometries [54-56] exist with different SPR wavelengths. Depending on how much overlap is allowed between SPR peaks of different nanoparticles, anywhere from a handful to dozens of detections could be carried out within the width of the visible spectrum.

While improvements are still needed in order to detect unamplified DNA, the techniques here could be easily integrated into more complex microfluidic devices, forming diagnostics capable of solving both major challenges in KS diagnosis: disease differentiation and starting with a solid sample. While in this work our samples are most illustrative of a biopsy sample after significant processing, in future work the system could be built to accept biopsy samples directly. A number of possible solutions exist for increasing the sensitivity of colorimetric nanoparticle-based detection, including the previously mentioned examples of detecting amplified RNA targets, such as vCyclin RNA, or using evanescent coupling into the particles to measure only scattered light. Additionally, lower limit detection could be possible by using nanoparticles at concentrations that are not visible to bind to target DNA, and then concentrating any resulting aggregates using a microfluidic device.

Another interesting case where multiplexed colorimetric detection based on metal nanoparticles could be applied is the detection of HIV and syphilis in the developing world, a problem recently tackled by Chin et al [26]. In this case, both diseases are treatable, but in pregnant women can become fatal to their children. Chin et al. develop a microfluidic ELISA chip to solve the problem and demonstrate amazing results with clinical samples. Here a multiplexed colorimetric solution could provide an easier readout in a similar device that could provide the patient with more confidence in the result.

Since therapeutics capable of controlling HIV, and thus in many cases KSHV, have been created the incidence rates of KS in the United States has decreased. However, in other areas of the world KSHV is still a major cause of cancer. Better diagnostics, potentially built utilizing the system described above, could be useful in diagnosing and allowing for subsequent treatment. The capability of multiplexed detections in one solution is particularly interesting in the case of differentiating between Kaposi's sarcoma and bacillary angiomatosis, as well as pyogenic granuloma by exclusion, where added difficulties besides multiplexing will arise from having to extract a bioanalyte from solid samples. In this case because of the limited sample size single solution multiplexed detection has an important advantage.

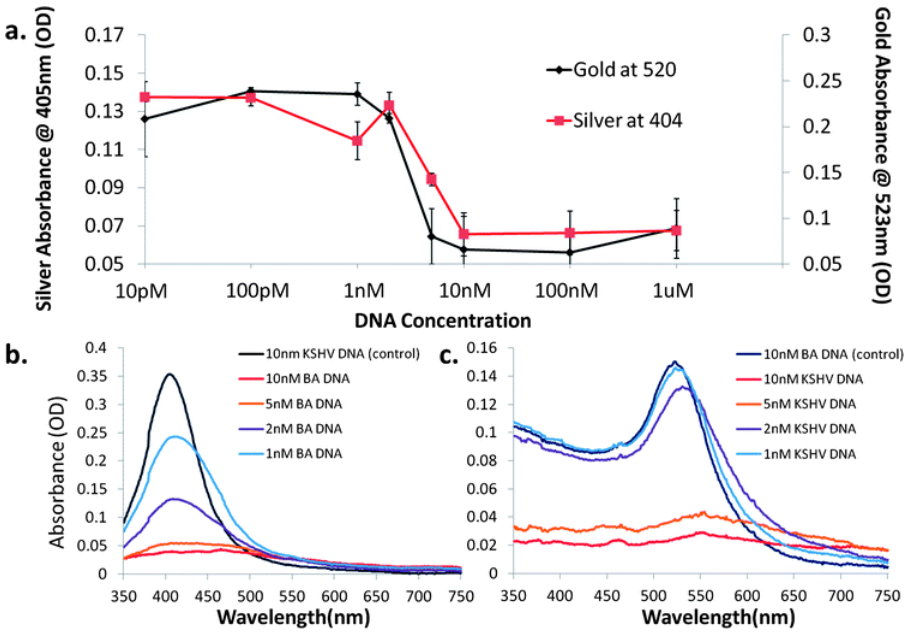

Fig. 6 (a) Sensitivity of both gold and silver nanoparticles conjugates. A color change was observed for silver solutions at 1nM DNA, and for gold nanoparticles at 2nM. (b) and (c) show the absorbance of the two systems between 1nM and 10nM, in the systems transition region. Note that this difference in sensitivity is likely because the silver nanoparticles are kept at a lower concentration while still providing a similar optical signal, a factor of the higher optical cross section of silver.

Here we have demonstrated work towards creating such a detection reaction that could later be integrated into a diagnostic device. We have shown that it is capable of detecting multiple targets, and that its limit of detection falls in line with similar work, and could be enhanced further using other known techniques. In future work we hope to integrate the reaction with biopsy-based detection, and solve both challenges involved in KS diagnosis.

5. Acknowledgements

This work was funded in part by the Clinical and Translational Science Center under NIH grant UL1 RR 024996. M. Mancuso would like to acknowledge a National Science Foundation Graduate Research Fellowship under Grant No. DGE-0707428. This work was performed in part at the Cornell NanoScale Facility, a member of the National Nanotechnology Infrastructure Network, which is supported by the National Science Foundation (Grant ECS-0335765) and at the Nanobiotechnology Center (NBTC), an STC Program of the National Science Foundation under Agreement no. ECS-9876771.

6. References

1. Hymes, K.B., et al., *Kaposi's sarcoma in homosexual men-a report of eight cases.* Lancet, 1981. **2**(8247): p. 598-600.
2. Friedman-Kien, A.E., *Disseminated Kaposi's sarcoma syndrome in young homosexual men.* J Am Acad Dermatol, 1981. **5**(4): p. 468-71.
3. Pitchenik, A.E., et al., *Opportunistic infections and Kaposi's sarcoma among Haitians:*

evidence of a new acquired immunodeficiency state. Ann Intern Med, 1983. **98**(3): p. 277-84.

4. *Update on Kaposi's sarcoma and opportunistic infections in previously healthy persons--United States.* MMWR Morb Mortal Wkly Rep, 1982. **31**(22): p. 294, 300-1.
5. Gallo, R.C., et al., *Isolation of human T-cell leukemia virus in acquired immune deficiency syndrome (AIDS).* Science, 1983. **220**(4599): p. 865-7.
6. Barre-Sinoussi, F., et al., *Isolation of a T-lymphotropic retrovirus from a patient at risk for acquired immune deficiency syndrome (AIDS).* Science, 1983. **220**(4599): p. 868-71.
7. Chang, Y., et al., *Identification of herpesvirus-like DNA sequences in AIDS-associated Kaposi's sarcoma.* Science, 1994. **266**: p. 1865-1869.
8. Gallo, R.C., *The enigmas of Kaposi's sarcoma.* Science, 1998. **282**(5395): p. 1837-9.
9. Nguyen, H.Q., et al., *Persistent Kaposi sarcoma in the era of highly active antiretroviral therapy: characterizing the predictors of clinical response.* AIDS, 2008. **22**(8): p. 937-45.
10. Eltom, M.A., et al., *Trends in Kaposi's sarcoma and non-Hodgkin's lymphoma incidence in the United States from 1973 through 1998.* J Natl Cancer Inst, 2002. **94**(16): p. 1204-10.
11. Ferlay J, et al. *Cancer Incidence and Mortality Worldwide: IARC CancerBase No. 10 [Internet]*. GLOBOCAN 2008 v1.2 2010 [cited 2011 11/15/2011]; Available from: http://globocan.iarc.fr].
12. Jemal, A., et al., *Global cancer statistics.* CA: A Cancer Journal for Clinicians, 2011. **61**(2): p. 69-90.
13. Mesri, E.A., E. Cesarman, and C. Boshoff, *Kaposi's sarcoma and its associated herpesvirus.* Nat Rev Cancer, 2010. **10**(10): p. 707-719.

14. Butler, L.M., et al., *Kaposi Sarcoma-Associated Herpesvirus (KSHV) Seroprevalence in Population-Based Samples of African Children: Evidence for At Least 2 Patterns of KSHV Transmission.* Journal of Infectious Diseases, 2009. **200**(3): p. 430-438.

15. Minhas, V., et al., *Early Childhood Infection by Human Herpesvirus 8 in Zambia and the Role of Human Immunodeficiency Virus Type 1 Coinfection in a Highly Endemic Area.* American Journal of Epidemiology, 2008. **168**(3): p. 311-320.

16. Martro, E., et al., *Comparison of human herpesvirus 8 and Epstein-Barr virus seropositivity among children in areas endemic and non-endemic for Kaposi's sarcoma.* Journal of Medical Virology, 2004. **72**(1): p. 126-131.

17. He, J., et al., *Seroprevalence of human herpesvirus 8 among Zambian women of childbearing age without Kaposi's sarcoma (KS) and mother-child pairs with KS.* J Infect Dis, 1998. **178**(6): p. 1787-90.

18. Tappero, J.W. and J.E. Koehler, *Bacillary Angiomatosis or Kaposi's Sarcoma?* New England Journal of Medicine, 1997. **337**(26): p. 1888-1888.

19. Caldwell, B., D. Kushner, and B. Young, *Kaposi's sarcoma versus bacillary angiomatosis.* Journal of the American Podiatric Medical Association, 1996. **86**(6): p. 260-2.

20. Berger Tg, T.J.W.K.A.L.P.E., *BAcillary (epithelioid) angiomatosis and concurrent kaposi's sarcoma in acquired immunodeficiency syndrome.* Archives of Dermatology, 1989. **125**(11): p. 1543-1547.

21. Tappero, J.W., et al., *Kaposi's sarcoma: Epidemiology, pathogenesis, histology, clinical spectrum, staging criteria and therapy.* Journal of the American Academy of Dermatology, 1993. **28**(3): p. 371-395.

22. Arlett, J.L., E.B. Myers, and M.L. Roukes, *Comparative advantages of mechanical biosensors.* Nat Nano, 2011. **6**(4): p. 203-215.

23. von Muhlen, M.G., et al., *Label-Free Biomarker Sensing in Undiluted Serum with Suspended Microchannel Resonators.* Analytical Chemistry, 2010. **82**(5): p. 1905-1910.

24. Zheng, G., X.P.A. Gao, and C.M. Lieber, *Frequency Domain Detection of Biomolecules Using Silicon Nanowire Biosensors.* Nano Letters, 2010. **10**(8): p. 3179-3183.

25. Mandal, S., J.M. Goddard, and D. Erickson, *A multiplexed optofluidic biomolecular sensor for low mass detection.* Lab on a Chip, 2009(DOI: 10.1039/b907826f).

26. Chin, C.D., et al., *Microfluidics-based diagnostics of infectious diseases in the developing world.* Nat Med, 2011. **17**(8): p. 1015-1019.

27. Martinez, A.W., et al., *Diagnostics for the Developing World: Microfluidic Paper-Based Analytical Devices.* Analytical Chemistry, 2009. **82**(1): p. 3-10.

28. Rosi, N.L. and C.A. Mirkin, *Nanostructures in Biodiagnostics.* Chemical Reviews, 2005. **105**(4): p. 1547-1562.

29. Yanik, A.A., et al., *Seeing protein monolayers with naked eye through plasmonic Fano resonances.* Proceedings of the National Academy of Sciences, 2011.

30. Storhoff, J.J., et al., *Homogeneous detection of unamplified genomic DNA sequences based on colorimetric scatter of gold nanoparticle probes.* Nat Biotech, 2004. **22**(7): p. 883-887.

31. Elghanian, R., et al., *Selective Colorimetric Detection of Polynucleotides Based on the Distance-Dependent Optical Properties of Gold Nanoparticles.* Science, 1997. **277**(5329): p. 1078-1081.

32. Thompson, D.G., et al., *Ultrasensitive DNA Detection Using Oligonucleotide−Silver*

Nanoparticle Conjugates. Analytical Chemistry, 2008. **80**(8): p. 2805-2810.

33. Chen, C.-K., C.-C. Huang, and H.-T. Chang, *Label-free colorimetric detection of picomolar thrombin in blood plasma using a gold nanoparticle-based assay.* Biosensors and Bioelectronics, 2010. **25**(8): p. 1922-1927.

34. Kalluri, J.R., et al., *Use of Gold Nanoparticles in a Simple Colorimetric and Ultrasensitive Dynamic Light Scattering Assay: Selective Detection of Arsenic in Groundwater.* Angewandte Chemie, 2009. **121**(51): p. 9848-9851.

35. Aslan, K., J.R. Lakowicz, and C.D. Geddes, *Nanogold Plasmon Resonance-Based Glucose Sensing. 2. Wavelength-Ratiometric Resonance Light Scattering.* Analytical Chemistry, 2005. **77**(7): p. 2007-2014.

36. Daniel, W.L., et al., *Colorimetric Nitrite and Nitrate Detection with Gold Nanoparticle Probes and Kinetic End Points.* Journal of the American Chemical Society, 2009. **131**(18): p. 6362-6363.

37. Storhoff, J.J., et al., *One-Pot Colorimetric Differentiation of Polynucleotides with Single Base Imperfections Using Gold Nanoparticle Probes.* Journal of the American Chemical Society, 1998. **120**(9): p. 1959-1964.

38. Reynolds, R., C.A. Mirkin, and R.L. Letsinger, *Homogeneous, Nanoparticle-Based Quantitative Colorimetric Detection of Oligonucleotides.* J. Am. Chem. Soc, 2000. **122**: p. 3795-3796.

39. Taton, T.A., C.A. Mirkin, and R.L. Letsinger, *Scanometric DNA Array Detection with Nanoparticle Probes.* Science, 2000. **289**(5485): p. 1757-1760.

40. Nam, J.-M., S.-J. Park, and C.A. Mirkin, *Bio-Barcodes Based on Oligonucleotide-Modified Nanoparticles.* Journal of the American Chemical Society, 2002. **124**(15): p.

3820-3821.

41. Nam, J.-M., C.S. Thaxton, and C.A. Mirkin, *Nanoparticle-Based Bio--Bar Codes for the Ultrasensitive Detection of Proteins.* Science, 2003. **301**(5641): p. 1884-1886.

42. Hill, H.D. and C.A. Mirkin, *The bio-barcode assay for the detection of protein and nucleic acid targets using DTT-induced ligand exchange.* Nat. Protocols, 2006. **1**(1): p. 324-336.

43. Shen, L., J.A. Hagen, and I. Papautsky, *Point-of-care colorimetric detection with a smartphone.* Lab on a Chip, 2012. **12**(21): p. 4240-4243.

44. Mudanyali, O., et al., *Integrated rapid-diagnostic-test reader platform on a cellphone.* Lab on a Chip, 2012. **12**(15): p. 2678-2686.

45. Veigas, B., et al., *Gold on paper-paper platform for Au-nanoprobe TB detection.* Lab on a Chip, 2012. **12**(22): p. 4802-4808.

46. Altschul, S.F., et al., *Gapped BLAST and PSI-BLAST: a new generation of protein database search programs.* Nucleic Acids Res, 1997. **25**(17): p. 3389-402.

47. Cai, X., et al., *Kaposi's sarcoma-associated herpesvirus expresses an array of viral microRNAs in latently infected cells.* Proceedings of the National Academy of Sciences of the United States of America, 2005. **102**(15): p. 5570-5575.

48. Koehler, J.E., et al., *Molecular Epidemiology of Bartonella Infections in Patients with Bacillary Angiomatosis–Peliosis.* New England Journal of Medicine, 1997. **337**(26): p. 1876-1883.

49. Murphy, C.J., et al., *One-Dimensional Colloidal Gold and Silver Nanostructures.* Inorganic Chemistry, 2006. **45**(19): p. 7544-7554.

50. Millstone, J.E., G.S. Métraux, and C.A. Mirkin, *Controlling the Edge Length of Gold*

Nanoprisms via a Seed-Mediated Approach. Advanced Functional Materials, 2006. **16**(9): p. 1209-1214.

51. Jin, R., et al., *Photoinduced Conversion of Silver Nanospheres to Nanoprisms.* Science, 2001. **294**(5548): p. 1901-1903.

52. Liu, M. and P. Guyot-Sionnest, *Mechanism of silver(I)-assisted growth of gold nanorods and bipyramids.* J Phys Chem B, 2005. **109**(47): p. 22192-200.

53. Zhang, J., et al., *Plasmon-Mediated Synthesis of Silver Triangular Bipyramids.* Angewandte Chemie International Edition, 2009. **48**(42): p. 7787-7791.

54. Sun, Y. and Y. Xia, *Shape-controlled synthesis of gold and silver nanoparticles.* Science, 2002. **298**(5601): p. 2176-9.

55. Hao, E., et al., *Synthesis of silver nanodisks using polystyrene mesospheres as templates.* J Am Chem Soc, 2002. **124**(51): p. 15182-3.

56. Zhou, J., et al., *Growth of tetrahedral silver nanocrystals in aqueous solution and their SERS enhancement.* Langmuir, 2008. **24**(18): p. 10407-13.

CHAPTER 4

DETECTION OF KAPOSI'S SARCOMA ASSOCIATED HERPES VIRUS NUCLEIV ACIDS USING A SMARTPHONE ACCESSORY

Kaposi's sarcoma (KS) is an infectious cancer occurring in immune-compromised patients, caused by Kaposi's sarcoma associated herpes virus (KSHV). Our vision is to simplify the process of KS diagnosis through the creation of a smartphone based point-of-care system capable of yielding an actionable diagnostic readout starting from a raw biopsy sample. In this work we develop the sensing mechanism for the overall system, a smartphone accessory capable of detecting KSHV nucleic acids. The accessory reads out microfluidic chips filled with a colorimetric nanoparticle assay targeted at KSHV. We calculate that our final device can read out gold nanoparticle solutions with an accuracy of .05 OD, and we demonstrate that it can detect DNA sequences from KSHV down to 1 nM. We believe that through integration with our previously developed components, a smartphone based system like the one studied here can provide accurate detection information, as well as a simple platform for field based clinical diagnosis and research.

Mancuso, M., Cesarman, E., Erickson, D. "Detection of Kaposi's Sarcoma Associated Herpes Virus Nucleic Acids Using a Smartphone Accessory," (Submitted)

1. Introduction

Kaposi's sarcoma (KS) is an opportunistic infectious cancer that first became widely known during the acquired immunodeficiency syndrome (AIDS) epidemic of the 1980s [1-4]. During this time period, the appearance of KS symptoms, red lesions on the skin, became signs that an individual was infected with human immunodeficiency virus (HIV), and KS itself became known as an AIDS-defining illness. As the battle against AIDS waged on, the introduction of highly active anti-retroviral therapy (HAART) helped reduce KS incidence [5]. Years later, however, HIV infected individuals still contract KS at a higher occurrence than when compared to the pre-AIDS era [6]. Considering its prevalence in HIV infected individuals, KS if often found in regions with high levels of AIDS. KS is the fourth leading cancer in sub-Saharan Africa, and in some countries, such as Uganda, is the most prevalent cancer in men [7-8].

The root cause of KS is the Kaposi's sarcoma herpesvirus (KSHV), also called human herpesvirus 8 (HHV-8) [9-10]. While the virus is often asymptomatic in healthy individuals, a number of populations, including those immune-compromised by HIV, are vulnerable to its symptoms and aggressive disease. The virus is commonly believed to be transmitted through saliva [11], and in some regions rapidly spreads beginning in childhood affecting large portions of the population, reaching seroprevalence of over 50% [8,12]. Like other herpesviruses, KSHV can establish a latent infection, and remains without causing any disease for life in most infected hosts, being necessary but not sufficient for KS development. Considering this, one of the biggest challenges in diagnosing KS involves having to detect KSHV in a biopsy sample and not simply a blood draw.

If typical hematoxylin and eosin (H&E) staining is applied to a KS biopsy section a number

of unique features can be observed, including many and large vascular spaces as well as high numbers of spindle cells thought to be of lymphatic endothelial origin [13-14]. However, due to the existence of similarly presenting diseases, such as bacillary angiomatosis (BA), identification of these features is frequently not sufficient for diagnosis of KS [15]. In modern hospitals, this is solved through immunohistochemistry staining for protein markers of KSHV, or through application of PCR for KSHV sequences.

However, neither of these techniques are readily adaptable for point of care field use situations in the developing world, where KS is most prevalent. Our long term goal is to create a biopsy diagnostic that can be used in this scenario, enabling the entire process from sample collection to diagnostic readout. In previous work, we began addressing this challenge to create point of care biopsy diagnostics for KS by creating a colorimetric nanoparticle based detection system, similar to the works of Thompson et al. [16] and Storhoff et al. [17-18], that was capable of detecting KSHV DNA [19]. However, one of the shortcomings of the system is that without laboratory technology, the test really can only be read out as a binary assay, and thus the amount of information it could provide was limited.

Recently, a number of mobile health technologies have been developed that seek to solve this problem of quantifiable point of care diagnosis. These devices take advantage of all of the computational, connectivity, display, and other functionality already built into a smartphone and use it to create better point-of-care devices. Further, they capitalize on the ubiquitous nature of smartphones, and the near universal ability to use them.

A number of papers have been published in the literature showing how smartphones can be used as field-portable microscopes [20-23], as colorimetric test strip readers [24-26], as rapid diagnostic test readers [27], for allergen detection [28], and even for label free detection [29].

These devices have proven extremely useful for portable imaging and in cases where diagnostic tests are commercially available. They advance the state of the art towards biochemical testing, yet are currently limited to only a few tests.

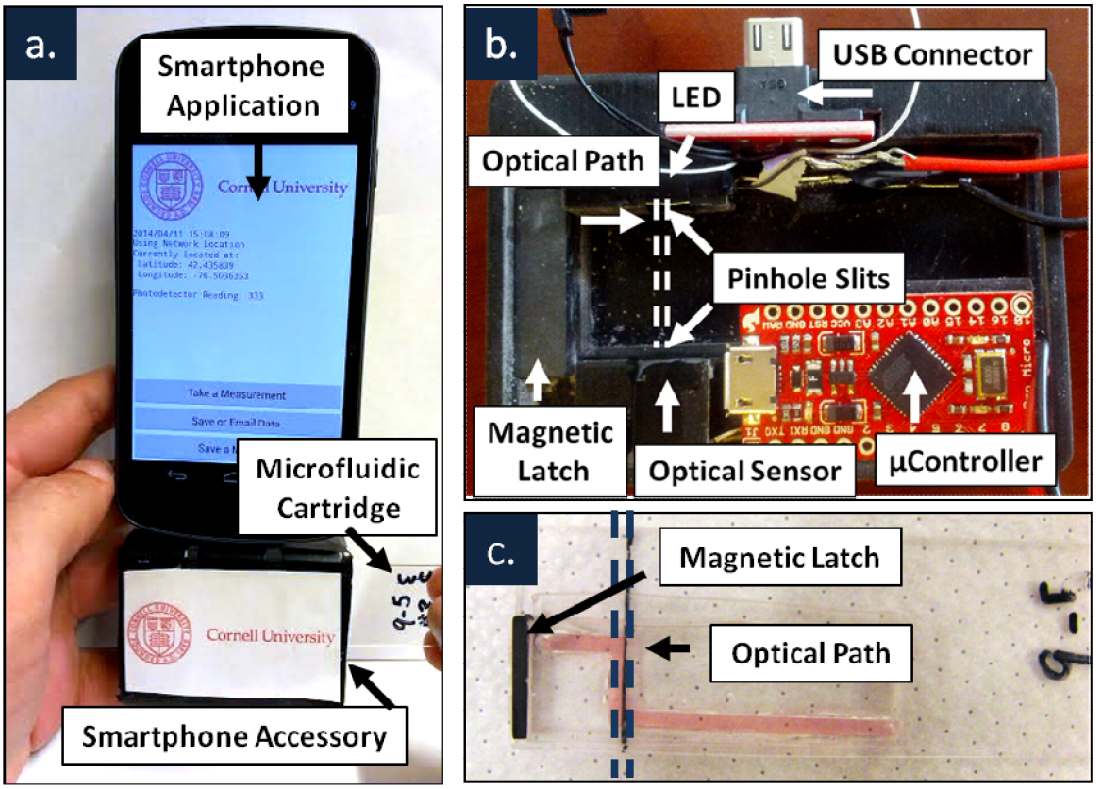

Fig. 1 (a) An image of the entire microfluidic smartphone system is shown including the Android application, the smartphone accessory, and a microfluidic chip being inserted. (b) The inside of the microfluidic chip is shown, with the light source and optical sensor out of position to include them in the image (normally they are across the width of the microfluidic chip). (c) An example microfluidic chip is shown illustrating the 1cm optical path the light travels through and the magnetic latch to help align the chip with the reader.

Mobile health technologies could be even further enhanced through their integration with additional microfluidic and lab-on-a-chip technologies. While many microfluidic devices exist in the literature [30-38], their penetration into commercial markets has been limited, as Chin et al.

well document in a recent review [39]. One of the challenges many of these devices face is the requirement for an expensive chip "reader" that contains electronics, optics, computation, display, and other functionality necessary for interrogating a test. If tests like these could ultimately be connected to smartphones, which already contain much of the required electronics, they could more easily penetrate into consumer markets.

In this work we create a smartphone accessory capable of measuring KSHV DNA. We develop a working accessory, a smartphone app, and disposable microfluidic chips, and show how we can detect KSHV DNA in a PDMS microfluidic chip. Overall, we show that we can measure nanoparticle solutions down to nanomolar concentrations, and detect KSHV DNA at similar levels. We hope that in the future the detection technology developed here will be integrated with other components, including syringe biopsy technology and solar thermal DNA amplification [40], to fully enable point-of-care biopsy based KS detection.

2. Experimental

Two smartphone accessories were created capable of reading out nanoparticle aggregation assays in standard laboratory cuvettes and 1cm long microfluidic channels. The cuvette based reader was used as a proof-of-concept device and to determine how to create the optical system. The rest of the work focuses on the microfluidic system, composed of a smartphone accessory, disposable microfluidic chips, and a smartphone app. The accessory connects to Android devices and is controlled by an Android app to obtain absorbance readouts across microfluidic chips. Figure 1 illustrates the system and its three components. The system was tested by reading out a gold nanoparticle aggregation assay developed for detecting KSHV DNA.

2.1 Software Development

The smartphone app was developed in Eclipse (Eclipse Foundation, Ottawa, Canada) for the Android platform (Google, Mountain View, CA). The code was written in java and used the Android SDK tools (Google, Mountain View, CA). The software was written to communicate with a USB accessory in accessory mode (host mode for the cuvette prototype), allowing the Android device to provide power for the smartphone accessory. When triggered via a button press in the app interface (see Figure 2), a signal is sent to the smartphone accessory requesting a read-out of the current absorbance. The app then receives this read-out, displays it to the user, and saves it in temporary memory. As results are collected, they can also be automatically tagged with user information, time stamps, and locations to provide relevance to the results. Figure 2c illustrates the process flow of the software.

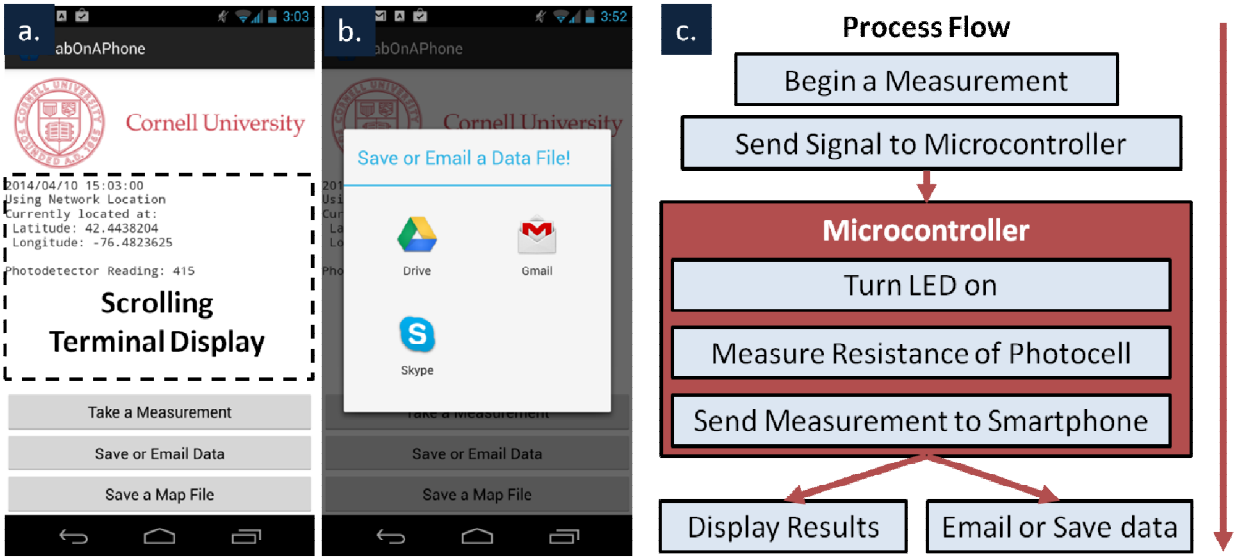

Fig. 2 (a) and (b) show screenshots of the Android application including where measurement output is recorded, how measurements are triggered, and additional functionality for emailing and saving data. (c) A flow chart illustrates the high level operation of the software running on both the Android phone and the Arduino microcontroller when a measurement is taken.

In addition to the app's core functionality, utilities were added to email results to other experimenters or medical professionals, to store results as text files on a connected Google Drive account, or even to create keyhole mark-up language files (KML files) that can be opened in Google Maps, Google Earth, or many other geographic applications (Figure 2b). Using these functions together, a simple database of test read-outs from numerous devices can be created, similar to that detailed in other work27. Eventually, records from similar accessories could be uploaded directly to patient's electronic medical records.

2.2 Optical Readout Circuitry

The accessory contains an LED light source at the peak wavelength of the nanoparticles resonance (520nm) and a photocell, placed across a 1cm gap where a sample is placed (Figure 2a). The photocell is connected via a pull-down resistor and measurements of the voltage drop across the photocell are made to determine luminosity. This results in an inversely proportional relationship between the output of the voltage measurement and the amount of light illuminating the photocell described by:

$$V = V_{in} \frac{R_{Photocell}}{R_{Photocell} + R_{Pull-down}} \qquad (1)$$

Where V is the voltage drop across the photocell, Vin is the power supplied to the resistor-photocell system, and RPhotocell and RPull-down are the resistance of the photocell and pull-down resistor respectively. If we also consider that the log of the resistance of a photocell is proportional to the log of the intensity of incident light given by:

$$\log R_I = -m \log I + k \qquad (2)$$

Where RI is the resistance for a given intensity, I, and m and k are constants relating to the specific photocell, and that absorbance through a medium varies according to the Beer-Lambert law given by:

$$T = \frac{I}{I_0} = 10^{-\varepsilon lc} \qquad (3)$$

Where T is transmitted light, I is transmitted Intensity, I0 is initial intensity, ε is molar absorptivity, l is the optical path length, and c is concentration then we can see that our voltage output is proposal to a sigmoid function of concentration:

$$V \propto V_{in} \frac{10^{-\varepsilon lc}}{10^{-\varepsilon lc} + R_{Pull-down}} \qquad (4)$$

By choosing the pull-down resistors resistance to make sure that typical concentrations fall in the middle of this range, a linear fit can then be used to describe the relation between voltage and optical density.

2.3 Cuvette Based Reader Proof of Concept and Circuitry

An accessory capable of reading out absorbance measurements across a cuvette was created to first demonstrate a smartphone's ability to measure nanoparticle absorbance and to test our optical component. This early prototype was based on an IOIO microcontroller board (Sparkfun, Boulder, CO) which enabled simple communication with the smartphone, but required external power and use of the USB Host interface. The microcontroller was connected to the LED and pull-down resistor and communicated measurement results with the smartphone.

All of the controlling electronics and measurement circuitry are house in a casing was printed using an Objet Connex500 3D printer (Stratasys, Eden Prairie, MN). This early prototype was battery powered, and connected via a USB cable to the Android phone.

2.4 Microfluidic Smartphone Accessory Design

The final microfluidic smartphone accessory can communicate with any modern Android smartphone or tablet, via power and communication through the devices µUSB port. The device consists of an 8MHz Pro Micro Arduino (Sparkfun, Boulder, CO), which controls the same type of LED and photodetector as used in the earlier prototype. The microcontroller connects to a male µUSB connector in order to draw power from and communicate with the smartphone. The entire system is enclosed in a black plastic case, printed similarly to the previous cuvette device, to block out ambient light.

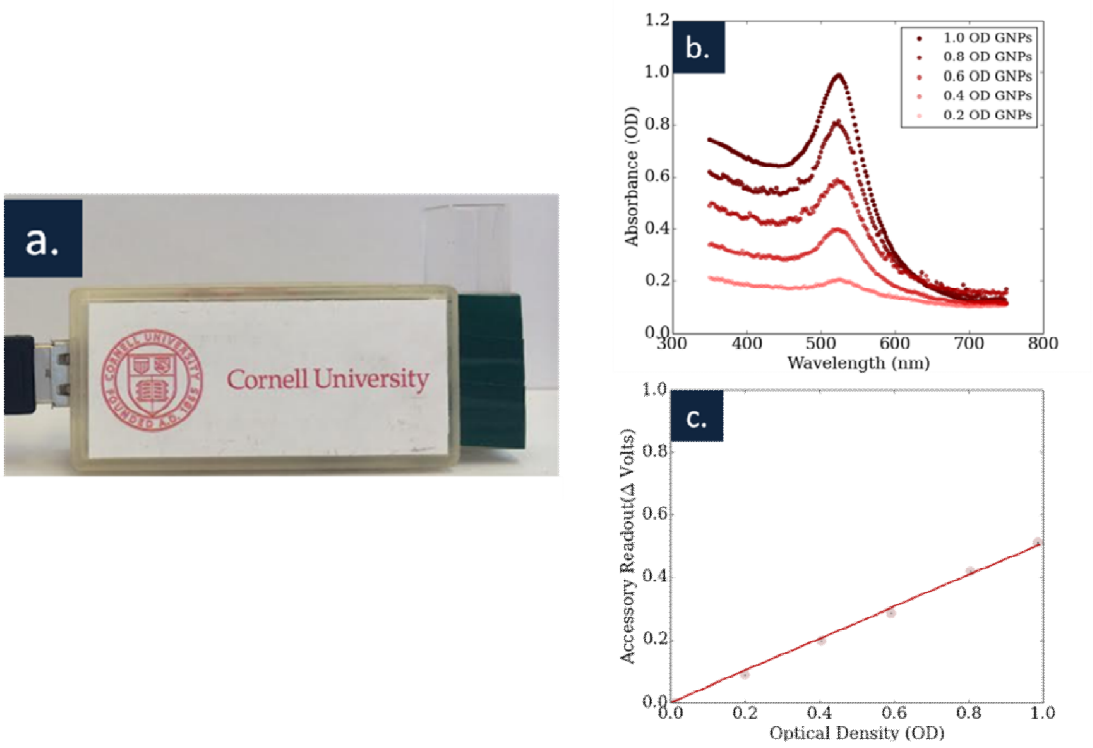

Fig. 3 (a) The cuvette based accessory is shown, along with (b) the spectrum of five gold nanoparticle solutions used to calibrate the accessory. (c) Shows the results of these initial experiments illustrating the changing accessory readout as a function of optical density. The sensitivity of the device was .5V/OD (R2 = .99).

The case holds the LED directly across from the photodiode, both behind approximately .5mm apertures. When a microfluidic chip is inserted, the path between the two components is filled with a 1cm path length fluidic channel full of a nanoparticle solution. A ceramic magnetic is also connected to the end of the accessory, useful for holding the microfluidic chip in alignment. The device can be seen in Figure 1b.

2.5 Microfluidic Chip Fabrication

Microfluidic devices were made of PDMS and glass and plasma-bonded together, as done extensively in the literature41-42. Briefly, a mold was made from laser cut polyacrylic using a VersaLASER laser cutter (Hobart Lasers, Kent, UK). This technique was chosen over the SU-8 or other microfabrication techniques because larger channels were desired for alignment, but similar microstructures could be easily integrated. The mold was then cast in PDMS, put under vacuum to removed trapped air bubbles, and baked overnight.

The resulting PDMS cast was cut from the mold, paying careful attention to leave 1mm of PDMS at the end of the sensing channel, enabling a thin interface for optical measurements along the width of the chip. Holes were punched at the inlet and outlet using and the PDMS channels and a microscope slide were then plasma treated in a Harrick Plasma Cleaner (Harrick Plasma, Ithaca, NY) for 30s. The treated surfaces were pressed together, and allowed an hour to bond. Small magnetic strips were then attached to the front of the microfluidic chips, helping with alignment once placed in the accessory. Fluidic actuation was provided using a syringe. A sample chip is shown in Figure 1c.

2.6 Gold Nanoparticle Assay

Short DNA sequences used as probes for KHSV DNA were designed previously using BLAST Primer Design43. Briefly, oligonucleotides specific to KSHV DNA that codes for vCyclin, were chosen. Gold nanoparticles were conjugated with oligonucleotides with 5' alkyl thiol groups, as in previous work. The nanoparticles had an average diameter of 15nm, a compromise between the higher sensitivity of larger particles, and the easier to work with nature and stability of smaller particles. 100 µL of 100 µM KSHV probes were added per 1mL of 3nM nanoparticle solution, and allowed to react overnight. Concentrated solutions of sodium phosphate and sodium dodecyl sulphate (SDS) were then added in order to bring the solution to 10mM and .01% concentrations, respectively, before another overnight period to reaction. Next, three additions of sodium chloride were added, resulting in concentration of 100mM, 200mM, and 300mM, each with 24 hours in between. This process worked to maximize the number of bound DNAs per particle, making more stable gold nanoparticle conjugates. After this, the resulting solution was spun down and resuspended in .01% SDS three times to remove unbound oligonucleotides. Sodium phosphate and Sodium chloride were then re-added to the final solution, resulting in final concentrations of 10mM Sodium Phosphate and 300mM Sodium chloride. Particles were then stable and usable for over a month.

2.7 Nanoparticle Sensitivity Characterization

Gold nanoparticle solutions of different concentrations were created in order to calibrate the device. 1 OD 15nm nanoparticles were diluted to concentrations of .8 OD, .6 OD, .4 OD, .2 OD,

and 0 OD. The absorbance of these solutions was measured using a SpectraMAX photometer (Molecular Devices, Sunnyvale, CA). These solutions were then placed in the cuvette based accessory, and read-out using an Android smartphone. Results were collected and plotted as a function of optical density. A best fit line was also calculated and plotted.

Similarly, these solutions were inserted into the microfluidic chip via syringe, and measured in order to determine the devices read-out at these absorbance levels. By mapping these results to the spectrometer's output, we created a calibration curve for the smartphone accessory. These curves were then used in further experiments to determine the optical density of solutions after the addition of KSHV DNA. Calibration curves were individually calculated for separate microfluidic chips. Measurements across chips was also collected, and plotted as a function of optical density, to show a measure of inter-chip repeatability.

2.8 Quantitative KSHV DNA Experiments

Gold nanoparticle conjugates were mixed with different concentrations of the target KSHV DNA sequence, ranging from 100pM, to 1μM. After 24 hours, the solutions were inserted into the smartphone accessory. The solutions were then measured by the smartphone, and the results were saved to the connected Google Drive for analysis. While solutions were given 24 hours to react in this work, we have carried out similar experiments at smaller volumes in as little as two hours in previous work [19], and there is literature precedent for faster times [18]. The main constraint here was due to diffusion in larger sample sizes prepared for multiple experiments. Resulting solutions were then measured using both our laboratory spectrometer and our microfluidic chip based system. Sensitivity results were calculated, and comparisons were made between the laboratory read-outs and our point of care readings.

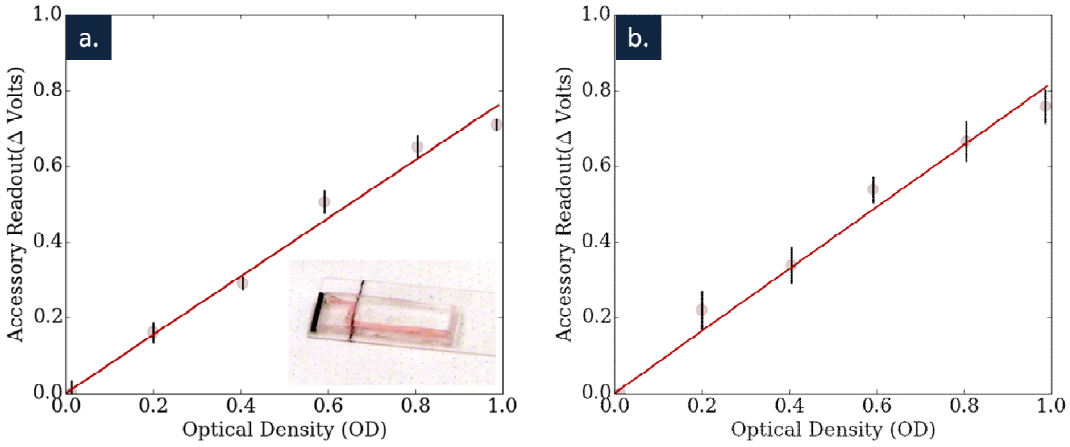

Fig. 4 (a) intra- and (b) inter- chip calibration and accuracy are shown for the microfluidic system. The data in (a) was then used as calibration data for the detection experiments. Within the single chip shown in (a) the sensitivity of the system was .77V/OD (R2 = .98) and across three chips the sensitivity was .82V/OD (R2 = .98), showing a high level of reproducibility.

3. Results and Discussion

3.1 Nanoparticle Sensitivity Results

Our cuvette reader and the results of our initial experiments using this system can be seen in Figure 3, along with the spectrum of the standard solutions used for calibration experiments. The change in voltage as a function of different optical density solutions can be seen. Error bars are shown, but difficult to see, as this initial system produced very tightly reproducible measurements, with standard deviations on the order of 2mV. The large volume of gold nanoparticle solution used insured that from the perspective of the sensor, the optical path was

always completely filled. The sensitivity of our reader, how much our voltage output changes with changing optical density, was roughly .5V/OD (R2 = .99). Considering this sensitivity, our error, Vin = 3.3V, and that our reading from the sensor is 10bit (1024 values), our sensor can read out optical densities to an accuracy of roughly .01 of an OD. This takes into account that the accessory has roughly 150 values in a 1OD range with our given sensitivity, and that our sensitivity is roughly on this scale (+/- 1 value). While this represents a best case value, even significantly less sensitive readings could be useful in point-of-care settings.

Figure 4 shows the resulting calibration data when comparing absorbance in our smartphone accessory to a commercial spectrometer. Both single and multiple chip measurements are shown, illustrating the intra- and inter- chip variations. As we can see from the results, our current prototype allows for highly repeatable measurements in a single chip and good measurements across chips. We believe that the additional variation between chips was the effect of channel alignment with the optical path, as well as uneven interfaces where the light enters and exits the chip. Together, these variations could account for unequal optical path lengths in the solution, as well as unequal scattering at the interfaces of the chip. We believe that both of these problems can be solved as we develop better techniques for repeatedly creating microfluidic chips that are measured along their width.

When considering the sensitivity of a single microfluidic chip, we actually calculate a higher sensitivity of .77V/OD (R2 = .98), a result of a smaller aperture and a different pull-down resistor. Considering again the accuracy of our device, we now have over 230 distinct voltage readings in our 1 OD range. However, because of alignment issues inserting a single chip repeatedly, the standard deviations of these measurements were approximately 9mV, larger than the voltage difference between values. Considering this, our microfluidic reader is accurate to

roughly .05 OD increments, though again this could be improved with better alignment, a more sensitivity detector, or more accurate read-outs of the photocell we use here.

While the sensitivity calculated across three chips was roughly the same (.82V/OD, R2 = .98) as to the single chip case above, the standard deviation increased to roughly 15mV, a result of alignment differences between chips.

3.2 KSHV Detection and Quantification

The results of our quantitative KSHV DNA detection experiments are summarized in Figure 5. Figure 5a shows the sensitivity of our assay, read out by both a spectrometer and our microfluidic smartphone accessory. Figure 5b compares the readouts of these two devices, showing a strong agreement between their results (best fit slope = .92, R2 = .96). Figure 5c shows the solutions tested at each point and how much KSHV DNA was added to each. Solutions with higher DNA concentrations were able to more completely react, and to do so more quickly, resulting in higher changes in absorbance at 520nm. Here our measurements use the calibration data for each of three microfluidic chips to calculate an optical density for these samples.

Our results indicate that with the current non-optimized system we can detect KSHV DNA down to nanomolar concentrations. However, other advances in nanoparticle based detection have been used to create much more sensitive systems than here (where a smaller amount of analyte results in a greater changed in OD), and if integrated with our smartphone accessory would likely yield more sensitive results.

4. Conclusions

Kaposi's sarcoma and other infectious diseases represent very real risks to human health both in the developing and developed world. The first step in treating these diseases is the identification of individuals affected, and to a lesser extent, how the disease is spreading. In this work we show how a smartphone based system can be cheaply and easily created to help solve both of these challenges. We demonstrate how the smartphone accessory we create can read out different concentrations of gold nanoparticles, as well as gold nanoparticle aggregation reactions that can be used to test for a number of different diseases.

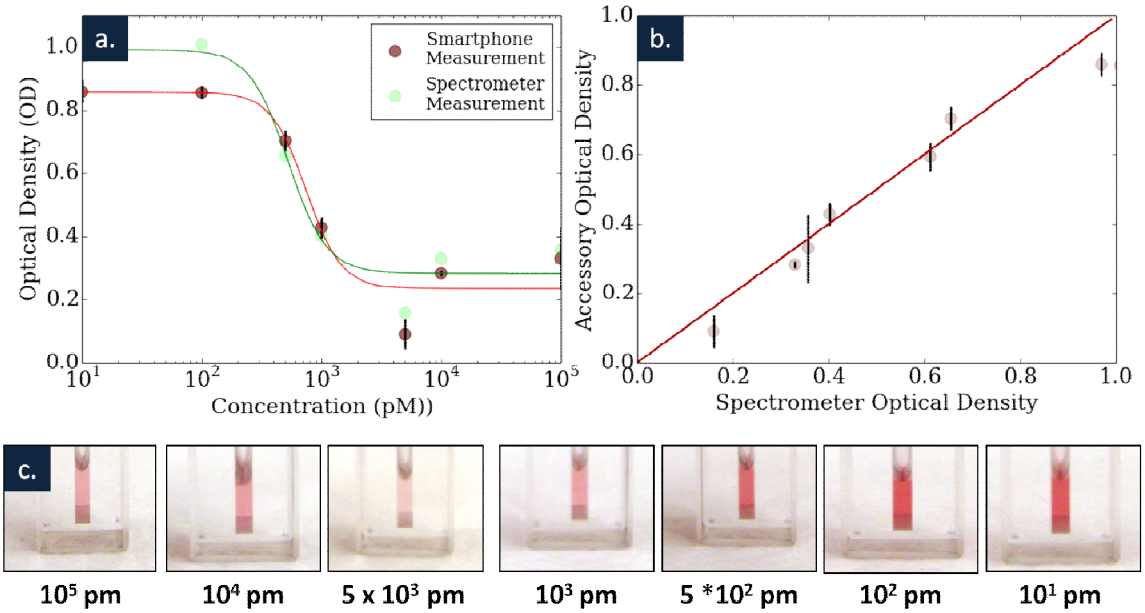

Fig. 5 (a) shows the optical density of the gold nanoparticle solution after the addition of 7 different concentrations of KSHV DNA. For concentration starting at 500pM and up to 1µM both the smartphone accessory and the spectrometer were able to detect changes in the color of the nanoparticle solution. (b) A plot of the optical density as determined by both the spectrometer and the smartphone accessory is shown, in comparison to a line representing parity. A best fit calculates an agreement of .92 between the two sets of measurements (R2 = .96). (c) Images of the seven different solutions are shown.

In this work, we demonstrate our system using DNA from KSHV. However, the same smartphone reader could be used with a number of other colorimetric reactions for things like Methicillin-resistant Staphylococcus aureus (MRSA) [44] and vitamin D levels [45]. Further, the same reader could be used in realms outside of healthcare, to detect things like heavy metal ions in water [46-49].

Unlike many devices in the literature that use the smartphone's camera, here we show how a simple standalone system can be built. While ultimately the inclusion of a separate optical detector can increase the cost and complexity of such a device, it has numerous advantages too. First, such a device isn't affected by changes in cameras between devices, allowing for more repeatable measurements, without any computational correction. Second, such a device could ultimately incorporate more sensitive detectors, creating diagnostics better suited for pathologies with low limits of detection. Lastly, one of the major challenges facing new diagnostics is often getting regulatory approval to launch such a device. While a camera based system is simple to implement, it is difficult to prove manufacturing control and repeatability when the sensor isn't directly coming from the diagnostic vendor, a problem that is circumvented through inclusion of a separate detector.

5. Acknowledgements

This work was partially supported by NIH-NIBIB under grant EB016803. M. Mancuso would like to acknowledge a National Science Foundation Graduate Research Fellowship under Grant No. DGE-0707428. This work was performed in part at the Cornell NanoScale Facility, a member of the National Nanotechnology Infrastructure Network, which is supported by the

National Science Foundation (Grant ECS-0335765) and at the Nanobiotechnology Center (NBTC), an STC Program of the National Science Foundation under Agreement no. ECS-9876771.

6. References

1. Pitchenik, A.E., et al., *Opportunistic infections and Kaposi's sarcoma among Haitians: evidence of a new acquired immunodeficiency state.* Ann Intern Med, 1983. **98**(3): p. 277-84.
2. CDC, *Update on Kaposi's sarcoma and opportunistic infections in previously healthy persons--United States.* MMWR Morb Mortal Wkly Rep, 1982. **31**(22): p. 294, 300-1.
3. Hymes, K.B., et al., *Kaposi's sarcoma in homosexual men-a report of eight cases.* Lancet, 1981. **2**(8247): p. 598-600.
4. Friedman-Kien, A.E., *Disseminated Kaposi's sarcoma syndrome in young homosexual men.* J Am Acad Dermatol, 1981. **5**(4): p. 468-71.
5. Eltom, M.A., et al., *Trends in Kaposi's sarcoma and non-Hodgkin's lymphoma incidence in the United States from 1973 through 1998.* J Natl Cancer Inst, 2002. **94**(16): p. 1204-10.
6. Nguyen, H.Q., et al., *Persistent Kaposi sarcoma in the era of highly active antiretroviral therapy: characterizing the predictors of clinical response.* AIDS, 2008. **22**(8): p. 937-45.
7. Jemal, A., et al., *Global cancer statistics.* CA: A Cancer Journal for Clinicians, 2011. **61**(2): p. 69-90.

8. Ferlay J, et al. *Cancer Incidence and Mortality Worldwide: IARC CancerBase No. 10 [Internet]*. GLOBOCAN 2008 v1.2 2010 [cited 2011 11/15/2011]; Available from: http://globocan.iarc.fr].

9. Cesarman, E., et al., *Kaposi's Sarcoma-associated Herpesvirus-like DNA sequences in AIDS-related body cavity-based lymphomas.* N Eng J Med, 1995. **332**: p. 1186-1191.

10. Chang, Y., et al., *Identification of herpesvirus-like DNA sequences in AIDS-associated Kaposi's sarcoma.* Science, 1994. **266**: p. 1865-1869.

11. Ablashi, D.V., et al., *Spectrum of Kaposi's sarcoma-associated herpesvirus, or human herpesvirus 8, diseases.* Clin Microbiol Rev, 2002. **15**(3): p. 439-64.

12. He, J., et al., *Seroprevalence of human herpesvirus 8 among Zambian women of childbearing age without Kaposi's sarcoma (KS) and mother-child pairs with KS.* J Infect Dis, 1998. **178**(6): p. 1787-90.

13. Tappero, J.W., et al., *Kaposi's sarcoma: Epidemiology, pathogenesis, histology, clinical spectrum, staging criteria and therapy.* Journal of the American Academy of Dermatology, 1993. **28**(3): p. 371-395.

14. Mesri, E.A., E. Cesarman, and C. Boshoff, *Kaposi's sarcoma and its associated herpesvirus.* Nat Rev Cancer, 2010. **10**(10): p. 707-719.

15. Tappero, J.W. and J.E. Koehler, *Bacillary Angiomatosis or Kaposi's Sarcoma?* New England Journal of Medicine, 1997. **337**(26): p. 1888-1888.

16. Thompson, D.G., et al., *Ultrasensitive DNA Detection Using Oligonucleotide−Silver Nanoparticle Conjugates.* Analytical Chemistry, 2008. **80**(8): p. 2805-2810.

17. Rosi, N.L. and C.A. Mirkin, *Nanostructures in Biodiagnostics.* Chemical Reviews, 2005. **105**(4): p. 1547-1562.

18. Storhoff, J.J., et al., *One-Pot Colorimetric Differentiation of Polynucleotides with Single Base Imperfections Using Gold Nanoparticle Probes.* Journal of the American Chemical Society, 1998. **120**(9): p. 1959-1964.

19. Mancuso, M., et al., *Multiplexed Colorimetric Detection of Kaposi's Sarcoma Associated Herpesvirus and Bartonella DNA using Gold and Silver Nanoparticles.* Nanoscale, 2013.

20. Greenbaum, A., et al., *Wide-field computational color imaging using pixel super-resolved on-chip microscopy.* Opt. Express, 2013. **21**(10): p. 12469-12483.

21. Greenbaum, A., U. Sikora, and A. Ozcan, *Field-portable wide-field microscopy of dense samples using multi-height pixel super-resolution based lensfree imaging.* Lab on a Chip, 2012. **12**(7).

22. Isikman, S.O., et al., *Field-portable lensfree tomographic microscope.* Lab on a Chip, 2011. **11**(13): p. 2222-2230.

23. Lee, M., O. Yaglidere, and A. Ozcan, *Field-portable reflection and transmission microscopy based on lensless holography.* Biomed. Opt. Express, 2011. **2**(9): p. 2721-2730.

24. Veigas, B., et al., *Gold on paper-paper platform for Au-nanoprobe TB detection.* Lab Chip, 2012. **12**(22): p. 4802-8.

25. Oncescu, V., D. O'Dell, and D. Erickson, *Smartphone based health accessory for colorimetric detection of biomarkers in sweat and saliva.* Lab on a Chip, 2013.

26. Shen, L., J.A. Hagen, and I. Papautsky, *Point-of-care colorimetric detection with a smartphone.* Lab on a Chip, 2012. **12**(21): p. 4240-4243.

27. Mudanyali, O., et al., *Integrated rapid-diagnostic-test reader platform on a cellphone.* Lab on a Chip, 2012. **12**(15): p. 2678-2686.

28. Coskun, A.F., et al., *A personalized food allergen testing platform on a cellphone.* Lab on a Chip, 2013. **13**(4): p. 636-640.

29. Gallegos, D., et al., *Label-free biodetection using a smartphone.* Lab on a Chip, 2013. **13**(11): p. 2124-2132.

30. Sharma, H., et al., *Unconventional Low-Cost Fabrication and Patterning Techniques for Point of Care Diagnostics.* Annals of Biomedical Engineering, 2011. **39**(4): p. 1313-1327.

31. Nguyen, D., et al., *Better shrinkage than Shrinky-Dinks.* Lab Chip, 2010. **10**(12): p. 1623-6.

32. Lutz, B., et al., *Dissolvable fluidic time delays for programming multi-step assays in instrument-free paper diagnostics.* Lab on a Chip, 2013.

33. Fu, E., et al., *Transport in two-dimensional paper networks.* Microfluidics and Nanofluidics, 2011. **10**(1): p. 29-35.

34. Lutz, B.R., et al., *Two-dimensional paper networks: programmable fluidic disconnects for multi-step processes in shaped paper.* Lab on a Chip, 2011. **11**(24): p. 4274-4278.

35. Fu, E., et al., *Chemical signal amplification in two-dimensional paper networks.* Sensors and Actuators B: Chemical, 2010. **149**(1): p. 325-328.

36. Nie, Z., et al., *Electrochemical sensing in paper-based microfluidic devices.* Lab on a Chip, 2010. **10**(4): p. 477-483.

37. Nie, Z., et al., *Integration of paper-based microfluidic devices with commercial electrochemical readers.* Lab on a Chip, 2010. **10**(22): p. 3163-3169.

38. Martinez, A.W., et al., *Diagnostics for the Developing World: Microfluidic Paper-Based Analytical Devices.* Analytical Chemistry, 2009. **82**(1): p. 3-10.

39. Chin, C.D., V. Linder, and S.K. Sia, *Commercialization of microfluidic point-of-care diagnostic devices.* Lab on a Chip, 2012. **12**(12): p. 2118-2134.

40. Jiang, L., et al., *Solar thermal polymerase chain reaction for smartphone-assisted molecular diagnostics.* Submitted, 2013.

41. Whitesides, G.M., *The origins and the future of microfluidics.* Nature, 2006. **442**(7101): p. 368-373.

42. McDonald, J.C. and G.M. Whitesides, *Poly(dimethylsiloxane) as a Material for Fabricating Microfluidic Devices.* Accounts of Chemical Research, 2002. **35**(7): p. 491-499.

43. Altschul, S.F., et al., *Gapped BLAST and PSI-BLAST: a new generation of protein database search programs.* Nucleic Acids Res, 1997. **25**(17): p. 3389-402.

44. Storhoff, J.J., et al., *Homogeneous detection of unamplified genomic DNA sequences based on colorimetric scatter of gold nanoparticle probes.* Nat Biotech, 2004. **22**(7): p. 883-887.

45. Farrell, C.-J.L., et al., *State-of-the-Art Vitamin D Assays: A Comparison of Automated Immunoassays with Liquid Chromatography–Tandem Mass Spectrometry Methods.* Clinical Chemistry, 2012. **58**(3): p. 531-542.

46. Hung, Y.-L., et al., *Colorimetric Detection of Heavy Metal Ions Using Label-Free Gold Nanoparticles and Alkanethiols.* The Journal of Physical Chemistry C, 2010. **114**(39): p. 16329-16334.

47. Knecht, M. and M. Sethi, *Bio-inspired colorimetric detection of Hg2+ and Pb2+ heavy metal ions using Au nanoparticles.* Analytical and Bioanalytical Chemistry, 2009. **394**(1): p. 33-46.

48. Darbha, G.K., et al., *Selective Detection of Mercury (II) Ion Using Nonlinear Optical Properties of Gold Nanoparticles.* Journal of the American Chemical Society, 2008. **130**(25): p. 8038-8043.

49. Lee, J.-S., M.S. Han, and C.A. Mirkin, *Colorimetric Detection of Mercuric Ion (Hg2+) in Aqueous Media using DNA-Functionalized Gold Nanoparticles.* Angewandte Chemie International Edition, 2007. **46**(22): p. 4093-4096.

CHAPTER 5

CONCLUSIONS

Over the course of my work I made significant improvements to polymer waveguide resonator biosensors and mobile health point of care diagnostics. In the following sections I outline my major accomplishments and challenges by project, as well as provide some information on future directions of the work.

5.1 Summary of Accomplishments

5.1.1 Nanoporous Polymer Ring Resonators for Biosensing

In this chapter, I presented novel work on how to create and use porous waveguide biosensors. These innovative devices used new materials to enable both simpler fabrication, and more importantly, structures that greatly increased the interaction between stored optical energy in the resonator and biomolecules in solution. The overall results showed a 40% increase in device sensitivity when compared to nonporous devices. Some of the key research accomplishments in this work included:

- Creation of porous polymer ring resonators using nanoimprint lithography, with top-down fabricated features down to 300nm, and chemically etched pores on the order of 50nm.

- Development of freeze fracture and electron microscopy techniques to observe and characterize the porous resonators
- Optimization of multiple chemistries to create pores small enough to avoid excessive light scattering while large enough to increase biomolecular interaction
- Development of clamp-on microfluidics which enabled biomolecule-waveguide interaction at small volumes while not mechanically or chemically destroying the delicate waveguide structures.
- Optical testing of the novel devices, demonstrating a 40% increase in overall sensitivity

5.1.2 Multiplexed Colorimetric Detection of Kaposi's Sarcoma Associated Herpesvirus and Bartonella DNA using Gold and Silver Nanoparticles

In Chapter 3, I demonstrated the development of a multiplexed colorimetric detection system for the differential diagnosis of two different pathogens. Gold and silver nanoparticle aggregation reactions were developed in such a way that the two reactions remained independent, with little cross-talk. The novel system was one of the first to use nanoparticles and colorimetric multiplexing, and was an instrumental stepping stone towards creating field portable diagnostics for Kaposi's Sarcoma. Some of the research highlights from this chapter included:

- Determination and development of suitable chemistries for creating color changing detection reactions sensitive enough to measure nanomolar concentrations of DNA.
- Optimization of bioconjugation chemistries in order to create independent reactions with little to no molecular cross-talk

- Demonstration of high specificity and nanomolar sensitivity of both reactions.
- Detection of KSHV and Bartonella DNA using the final system

5.1.3 Detection of Kaposi's Sarcoma Herpes Virus DNA Using a Mobile Health Smartphone Accessory

In Chapter 4, work was presented on quantitative diagnosis of Kaposi's sarcoma DNA using a smartphone accessory. In this work we demonstrated for the first time how colorimetric gold nanoparticle aggregation reactions could be read out using a smartphone accessory. This work was one of the first to create an optical smartphone accessory capable of reading out a biodetection reaction and unique from similar previous works in its exclusion of the smartphone camera. We demonstrated the ability to detect KSHV DNA down to nanomolar levels in microfluidic chips. Some of our key breakthroughs included:

- Development of a smartphone powered optical detection accessory that could read out colorimetric reactions
- Calibrations tests showing the sensitivity and resolution of our prototype
- Sensing experiments showing smartphone detection of KSHV DNA down to nanomolar concentrations
- Additional features including geo-tagging and map-creation that can enable new epidemiologic studies.

5.2 Future Directions

5.2.1 Nanoporous Polymer Ring Resonators for Biosensing

At the conclusion of our work on porous polymer ring resonators, we had developed a polymer system capable of achieving higher sensitivities through unique materials. Due to the fabrication and materials selected, we could have continued developing on our devices to create flexible, wearable optical biosensors. An illustration of what such a sensor could have looked like is shown in Figure 1. Sensors like these ultimately could be used by the chronically ill to measure disease status, by early response workers to measure potential threats, and by soldiers to detect weaponized pathogens. While ultimately I chose to pursue a different direction with my dissertation work, polymer waveguide biosensors is still a very active area of research, and our work[1] has already been cited numerous times as of this writing.

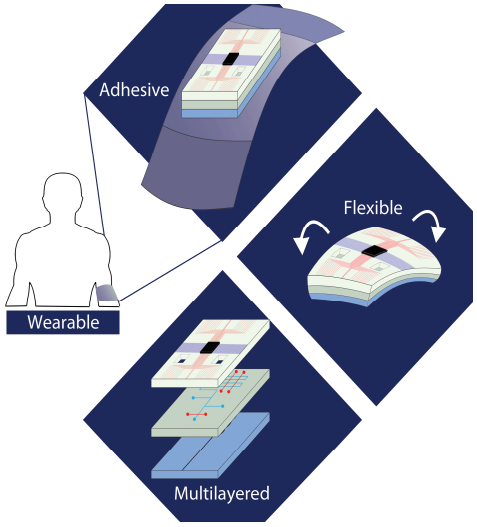

Fig. 1 A diagram illustrates what our porous polymer waveguides could one day ultimately be built into. Combining flexible polymer optical layers with similar fluidics and electronics could one day be used to create form-fitting biosensor wearables.

5.2.2 Multiplexed Colorimetric Detection of Kaposi's Sarcoma Associated Herpesvirus and Bartonella DNA using Gold and Silver Nanoparticles

In Chapter 3, the development of a colorimetric detection scheme for Kaposi's sarcoma associated herpesvirus was described. This work was performed at the start of a new collaboration with Professor Ethel Cesarman, and has gone on to result in a number of new projects, including the following work in my thesis. Overall, the aim of our collaboration is to create point of care diagnostics for KS that complete the whole process from sample collection, to entry into a patient's electronic medical record. Figure 2 outlines the concept behind this idea.

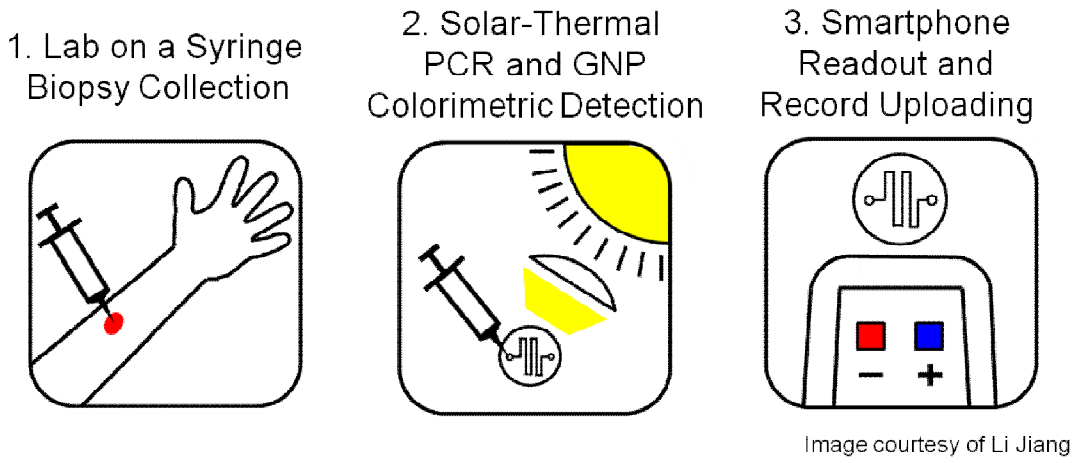

Fig. 2 The concept behind our broader point of care KS diagnostic is shown. A sampel is collected using a biopsy syringe, amplified with solar-thermal PCR and fed into the color change reaction developed in Chapter 3, and ultimately read out using a smartphone based system as in Chapter 4.

The first part of this work, the development of a method to collect a biopsy and extract DNA from it, has been tackled by the Cesarman lab. There, they are developing a method where the

biopsy samples can be lysed using only minimal chemicals and external infrastructure in a way that produces DNA ready for amplification in step 2. I've also made small contributions in this area, providing early vision for this part of the project, and creating prototypes of what a system capable of doing steps 1 and 2 might look like. This early prototype is shown in Figure 3, and consists if a biopsy needle and a syringe attached in such a way that a sterile sample can be collected and fed right into a microfluidic chip.

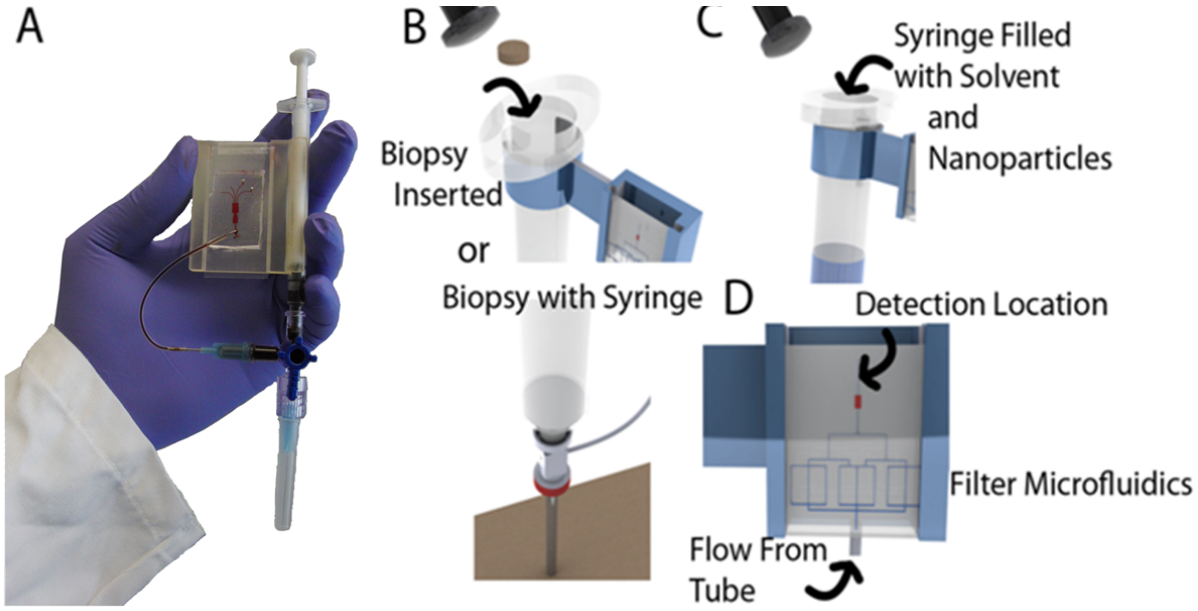

Fig. 3 (A) Shows a prototype lab on a syringe device, demonstrating how a sample can be collected using a syringe, and ultimately injected into a microfluidic chip, where a colorimetric detection reaction can occur. (B) Illustrates two ways in inserting a biopsy sample followed by (C) showing the addition of necessary reagents. (D) Shows the final microfluidic chip, and a detection location where a color change can be observed.

In addition to the colorimetric detection already described in Chapter 3, the second part of this overall system also has the ability to amplify DNA using solar-thermal polymerase chain

reaction. This system was ultimately designed and published on by my colleague, Li Jiang, who I collaborated closely with over the duration of the project[2]. I contributed to this project providing some of the earliest engineering designs for the system (shown in Figure 4 along with Jiang's final system) and help with the biochemical aspects of the project. While the results of this work are ultimately those of Li Jiang, for the sake of the project as a whole it's worth noting that the final PCR system can work on samples with as little as 100 copies per µL.

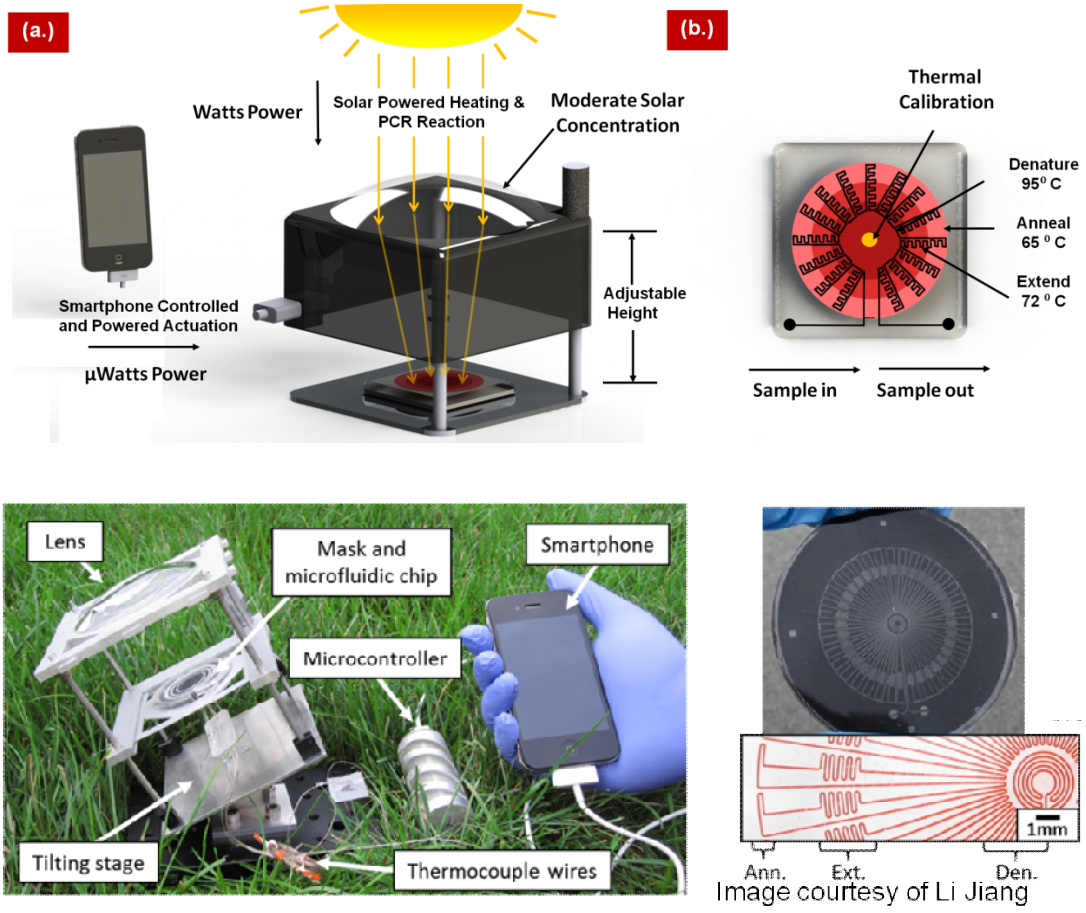

Fig. 4 (top) The concept for our solar thermal PCR is shown. A smartphone us used to control the device and read out temperatures, while most of the power required for the amplification comes from the sun. The microfluidic chip used with the system is shown on the right. (bottom) The final working system is shown used in the field, along with a close-up of the microfluidic chip [2].

The next steps for the first two parts of this system involve field testing in sub-Saharan Africa, scheduled for February 2014. My colleagues will be taking parts of the system to two different field locations to see if preliminary results can be obtained using our device. Following these tests, the goal is to conduct larger scale clinical trials, and see if our technology can one day ultimately be used in the field.

5.2.3 Detection of Kaposi's Sarcoma Herpes Virus DNA Using a Mobile Health Smartphone Accessory

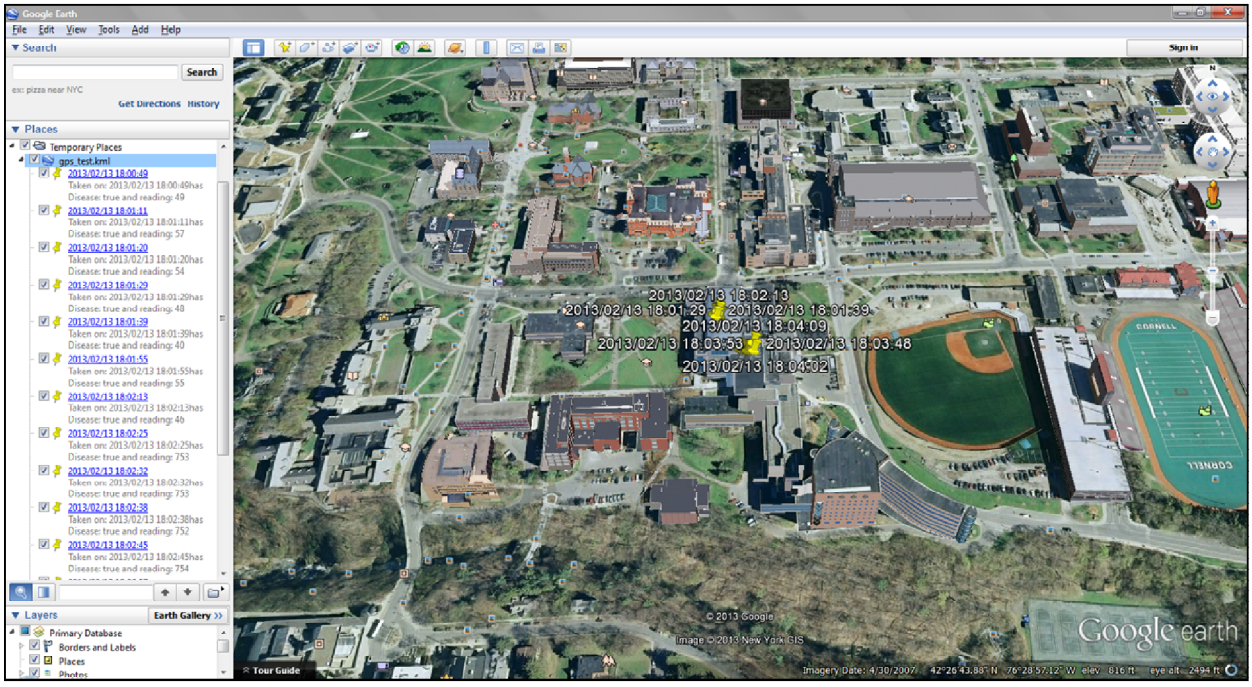

Fig. 5 A map file is shown with multiple readouts of different KSHV levels. Ultimately, epidemiologic maps can be created that could be used to better manage and triage disease on a population level.

In Chapter 4 of this dissertation, results were presented on smartphone based readout of our KSHV assay. Ultimately this system will be used as the final part of our overall KSHV field diagnostic, as described above. In addition to the results presented in the chapter, one additional advantage smartphones provide is their ability to add extra information to diagnostics tests. One example, geo-tagging, can be used to create non-identifying epidemiologic information as tests are recorded. Figure 5 shows an example KML file created using our smartphone accessory and app, mapping recordings of KSHV levels to different locations. Other examples include adding information through the smartphone interface collected via physical examination, or uploaded through other devices. In its current form, the future of this work will ultimately be its integration into the complete system.

More exciting to me than the initial work alone, during the course of my research on smartphone based biochemical diagnosis, colleagues and I began developing a whole collection of different uses for such technology. This original work acted as a springboard for a number of other research projects colleagues of mine lead, including smartphone accessories to measure sweat pH [3], cholesterol levels [4], and vitamin D levels[5]. The more we looked, the more it became clear that mobile health technologies are going to be much more than simply part of one diagnostic. Figure 6 illustrates one of these new systems a colleague, Seoho Lee, developed to detect vitamin D levels using a smartphone [5]. Going forward, my work on smartphone diagnostics will hopefully fuel many other researchers, leading to all sorts of applications ranging from simple tests for things like ovulation, to home use cancer diagnostics. Attached at the end of this document is an appendix of some tests which could be modified to work on a smartphone.

Fig. 6 A smartphone accessory for vitamin D is shown, based on using the smartphone camera to detect a colorimetric reaction [5].

5.4 Concluding Remarks

As described in Chapter 1, I believe one day mobile health accessories will be used as the first step in healthcare, reducing the burden on doctors and providing an unprecedented level of distributed healthcare. As outlined in my work, there exists numerous opportunities to create and commercialize advanced diagnostics for home-use. I hope that my contributions to the field, in summary the adoption of gold nanoparticle diagnostics to smartphone accessories, will be expanded upon by others, and one day inspire a new generation of portable diagnostics.

5.5 References

1. Mancuso, M., J.M. Goddard, and D. Erickson, *Nanoporous polymer ring resonators for biosensing.* Optics Express, 2012. **20**(1): p. 245-255.
2. Jiang, L., et al., *Solar thermal polymerase chain reaction for smartphone-assisted molecular diagnostics.* Scientific Reports 2014.
3. Oncescu, V., D. O'Dell, and D. Erickson, *Smartphone based health accessory for colorimetric detection of biomarkers in sweat and saliva.* Lab on a Chip, 2013. **13**(16): p. 3232-3238.
4. Oncescu, V., M. Mancuso, and D. Erickson, *Cholesterol testing on a smartphone.* Lab on a Chip, 2014. **14**(4): p. 759-763.
5. Lee, S., et al., *A smartphone platform for the quantification of vitamin D levels* Submitted, 2014.